



โครงการ
การเรียนการสอนเพื่อเสริมประสบการณ์

ชื่อโครงการ	การศึกษาผลของความหนาแน่นพลาสมาต่อเครื่องเร่งอนุภาคเวคฟิลด์ในสนามแม่เหล็กแนวแกนด้วยระเบียบวิธีปาร์ติเคิลอินเซลล์	
	Study of Plasma Density Effects on Laser Plasma Wakefield Accelerator in Presence of Axial Magnetic Field using Particle-in-cell Method	
ชื่อนิสิต	วรากร ภูสุวรรณ	เลขประจำตัว 5933441823
ภาควิชา	ฟิสิกส์	
ปีการศึกษา	2562	

คณะวิทยาศาสตร์ จุฬาลงกรณ์มหาวิทยาลัย

Senior Project

Study of Plasma Density Effect on Laser Plasma Wakefield
Accelerator in Presence of Axial Magnetic Field
using Particle-in-cell Method

Waragon Phusuwan

Student's ID: 5933441823

Advisor

Asst. Prof. Dr. Boochoat Paosawatanyong

Department of Physics

Faculty of Science, Chulalongkorn University

2nd Semester, Academic year 2019

Project Name Study of Plasma Density Effect on Laser Plasma Wakefield Accelerator in Presence of Axial Magnetic Field using Particle-in-cell Method

Author Waragon Phusuwan


Advisor Asst. Prof. Dr. Boonchoat Paosawatanyong


Department Physics

Academic Year 2019

This project serves as a part of curriculum for Bachelor of Science, Physics Major, Faculty of Science, Chulalongkorn University for academic year 2019.

The members appointed to examine the project of Waragon Phusuwan find satisfactory and recommend that it accepted.


..... Chairperson
(Assoc. Prof. Dr. Surachate Limkumnerd)


..... Examiner
(Assoc. Prof. Dr. Rattachat Mongkolnavin)


..... Advisor
(Asst. Prof. Dr. Boonchoat Paosawatanyong)

Project Name	Study of Plasma Density Effect on Laser Plasma Wakefield Accelerator in Presence of Axial Magnetic Field using Particle-in-cell Method
Author	Waragon Phusuwan
Advisor	Asst. Prof. Dr. Boonchoat Paosawatanyong
Department	Physics
Academic Year	2019

Abstract

In this study, dependence of energy distribution of electrons inside laser plasma wakefield accelerator (LWFA) on factors such as laser's strength, plasma density and axial magnetic field are investigated. LWFAs with hydrogen plasma are simulated using freeware PConGPU on NARIT's CHALAWAN. Results show that electron blowout inside LWFA is in different mode depending on laser's strength. Energy peak occurs for plasma density range of 10^{24} m^{-3} to 10^{25} m^{-3} which identifying electrons trapping and acceleration. Energy peaks have common characteristic that the generation of peak and peak deceleration occur for approximately the same time interval. Higher plasma density's energy peak occurs at lower energy while having more particles in the peak. Next, the background axial magnetic effect on energy distribution is observed. The results conclude that some range of magnetic field can be used to enhance LWFAs.

Acknowledgment

The study will not be successful if not for helps and supports both physically and mentally from friends and family. Educational and knowledge support from advisor and laboratory's master student. I hereby express my gratitude toward my lab's senior Chatchai who had helped me numerous times. Gratitude toward my advisor Asst. Prof. Dr. Boonchoat Paosawatanyong who provided opportunities to learn many new things and accepted my wish to investigate this topic. Gratitude toward Assoc. Prof. Dr. Surachate Limkumnerd and Assoc. Prof. Dr. Rattachat Mongkolnavin as examination committee. Finally, I acknowledge all contributors to the open-source code PConGPU for enabling our simulations.

To those who have helped me in any way in the past, thank to you all that I can keep moving.

Gratitude

Waragon Phusuwan

Contents

CHAPTER ONE: Introduction.....	1
1.1 Background and Motivation.....	1
1.2 Aims and Objective of the Study.....	3
1.3 Significant of the Study	4
1.4 Scope of the Study	4
CHAPTER TWO: Literature Review.....	5
2.1 Wave-Induced acceleration.....	5
2.2 Toy model of wave-induced acceleration.....	7
2.3 Plasma Wakefield Accelerator and Laser Plasma Wakefield Accelerator.....	9
2.4 Enhancing wakefield accelerator	13
2.5 Enhancing wakefield accelerator by longitudinal magnetic field.....	14
2.6 Plasma density effects on wakefield accelerators.....	16
2.7 Particle-in-Cell method.....	19
CHAPTER THREE: Research Methodology	20
3.1 Research Design	20
3.2 Gantt chart	22
CHAPTER FOUR: PIconGPU.....	23
4.1 Overview.....	23
4.2 Parameter file	23
4.2.1 density.param.....	23
4.2.2 grid.param	25
4.2.3 laser.param	25
4.2.4 fieldsolver.param.....	26
4.2.5 species.param.....	27
4.2.6 speciesDefinition.param	29
4.2.7 fieldbackground.param	30
4.3 Configuration file.....	31

4.3.1 General Configuration.....	31
4.3.2 Plugins Configuration	32
4.3.3 Program Parameters.....	34
4.4 Simulation Setup	35
CHAPTER FIVE: RESULTS AND DISCUSSION	38
5.1 Electrons and ions motion inside laser-plasma wakefield accelerator.....	38
5.2 Plasma Density Effects on Blowout Radius and Shape	42
5.3 Plasma Density Effects on Electrons Acceleration.....	44
5.4 Axial Magnetic field's influence on electron acceleration	54
5.5 Discussion	55
5.6 Summary.....	56
APPENDIX A: Example of .param file.....	58
A.1 laser.param	58
A.2 density.param.....	64
A.3 grid.param.....	68
APPENDIX B: Example of .cfg file	71
Bibliography	77

CHAPTER ONE: Introduction

1.1 Background and Motivation

Acceleration is the rate of change in velocity of interested point. It is first formulated in physics through Newton's law of motion. Particles subjected to non-zero net force manifest the acceleration and vice-versa. Assertion of force upon a particle will accelerate or decelerate it and by doing so, people can increase or decrease the particle's kinetic energy. Such an idea is the basis for particle acceleration. There are numerous methods to bestow the particle energy upon a particle. However, achieving high kinetic energy is not the only thing needed to be considered. To utilize most part of accelerated particles, they should be confined to a monoenergetic beam which can be achieved using electromagnetic field like conventional particle accelerators. Therefore, particle accelerators normally refer to either electrostatic or electrodynamic particle accelerator. Conventional particle accelerators use the electric field to accelerate charge particles in preferred direction then confine them using magnetic field. The largest particle accelerator is European Organization for Nuclear Research's Large Hadron Collider or LHC, which achieved the collision of 7 TeV total energy, in their first experiment in 2010. LHC was upgraded in 2014 and then restarted in 2015. After restarting, it can produce 13 TeV total collision energy and the highest world record up until today. At the end of 2018, LHC underwent a further upgrade. Despite LHC overall achievements, some physicists seek for a new method to accelerate particle in short distance. Plasma – based acceleration is one candidate to solve this problem of distance.

Plasma – based particle acceleration is the field of interest for long time. First relevant idea, cosmic ray acceleration with comoving electromagnetic field, is investigated by Fermi and McMillan in 1960s (1). After the invention of laser in 1960, the area of laser – particle accelerations are being thoroughly investigated. Several mechanisms to utilize laser in particle acceleration are proposed in 1970s. Y. W. Chan studied electron acceleration in order of 40 MeV by comoving relativistic electron beam and laser and R. B. Palmer (2) discussed electron acceleration of laser moving through the helical magnetic field. W. J. Willis proposed an idea of positive – ion acceleration using electron beam modulated by laser light. In 1979, Tajima and Dawson proposed an idea of laser – electron acceleration which is called laser-plasma wakefield accelerator (LWFA) later. PWFA is like an extension of Chan and those of Fermi and McMillan, the laser tackles off the electron in plasma with its ponderomotive force and create a volume of space charge which eventually generates a moving wave of plasma density and accelerate the electrons with ultra – high acceleration gradient. Wakefield accelerations provide an affordable and compact accelerator for various applications in high – energy physics as well as in medical and industrial fields.

After pioneer work of Tajima and Dawson, plasma wakefield has been investigated through experimental and theoretical means. Experimental studies of wakefield accelerator began at University of

Chicago, Los Angeles (UCLA) by Prof. Chan Joshi in 1984 (3), collaborating Dawson and Katsouleas. To the extent of author's knowledge, wakefield accelerator did not gain much interest from physicists due to its requirement on advance instruments such as high – power laser source (or supercomputer for case of simulations). However, there has been several laboratory experiments on wakefield accelerator producing recognizing results and numerous publications on experimental wakefield accelerator. For the other side of investigation, the theoretical study, wakefield acceleration are discussed in various topic relate to control of accelerator such as the effect of plasma density on the wake and energy gain, evolution of wakefield, self – injection (4), and hosing instability. Although the theoretical problems of wakefield accelerator are obvious, we have not yet found the theory completely describing everything inside real wakefield acceleration which are closely relate to plasma oscillation. Wakefield's problems in real situation arise from nonlinearity. Since wakefield is, actually, an oscillatory response of perturbed plasma, the linear plasma theory makes good descriptions for weak perturbation. However, to maximize the acceleration gradient in wakefield accelerator, we are forced to implement wakefield accelerator in highly perturbed way and by doing so, linear theory will not be enough to describe wakefield in that state.

After wakefield accelerator reach blowout regime, nonlinear oscillatory dynamics in plasma became topic of interest for plasma scientists. The nonlinear theory of plasma oscillation will help physicists in parameter scan for construction of optimum wakefield accelerator. Nonlinear models existed at that time are only few and cannot be implemented to the real accelerator. In 1956, the pioneer work on nonlinear theory of plasma oscillation by Polovin and Akhiezer (5), with 1 – D nonlinear cold plasma wave dynamics including relativistic effect is developed. After one-dimensional theory is developed, there is not much progress on 2 or 3 – dimensional plasma oscillations associated with waves of phase velocity close to speed of light. Since multidimensional plasma oscillatory motion is much more complicate due to relativistic mass effect and trajectory crossing. Trajectory crossing is one of the reasons prohibiting linear theory in real wakefield accelerators (being multidimensional accelerator) since linear plasma theory generally assumes no crossing laminar fluid. The most recent work on the nonlinear theory of plasma wakefield accelerators is by Wei Lu (4). The theory applications to wakefield accelerators are gathered in his doctoral dissertation.

Since there is no theory for multidimensional nonlinear plasma oscillation with relativistic effect, researcher tends to investigate related phenomenon using experiment or plasma simulation. The famous numerical simulation method in plasma physics is called Particle – In – Cell method (or PIC). There are many program/software utilizing PIC for plasma simulation both for commercial and non-commercial purposes such as OSIRIS, COMSOL, CUBESAT and PIConGPU. PIConGPU is the package of program in Linux for PIC plasma simulation accounting for relativistic effect, but instead of running computation on RAM, PIConGPU execute the command on Graphic Processing Unit (GPU) for faster simulation. The package also include laser – plasma interaction which is another active field in plasma physics. Laser on PIConGPU can

be used to create wakefield accelerator by the mechanism proposed by Tajima. Such an accelerator is called Laser – Wakefield Accelerator (LWFA) and its mechanism does not differ much from PWFA.

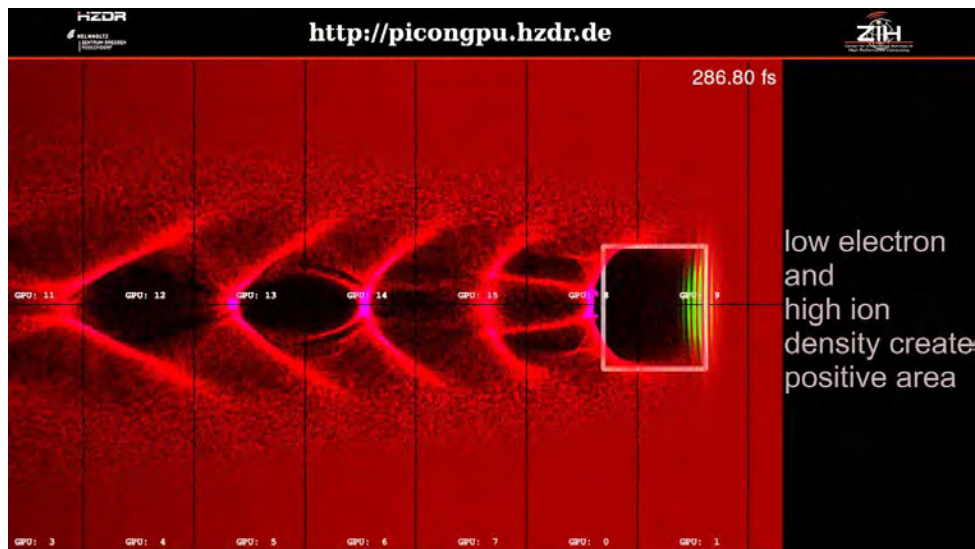


Fig 1.1 Snapshot of PIC simulation in package PICongGPU

source: https://www.youtube.com/watch?v=lgxVYL_pslI&t=71s

Fig 1.1 shows information on electrons density in which intensity of color defines denser area. In this simulation, the laser's electric field magnitude is shown in yellow. The stripes of yellow color shows information of laser wave phase.

Several research on configuration effects on wakefield acceleration are widely investigated both on experiment and simulation study in order to find optimum condition/parameters for wakefield acceleration. Electron trapping and energy gain in LWFA can be enhanced by externally applied longitudinal static magnetic field⁸ while background plasma density directly affects the acceleration gradient. Magnetic field and background plasma density both affect the output of wakefield accelerator as mentioned, but those researches are conducted separately, so there is a remaining question: What is the effect of these parameters on each other? In this undergraduate research, the author aims to find the effect of background magnetic field on the optimum plasma density for wakefield accelerators. The study is conducted mainly on simulation package PICongGPU which is Particle – In – Cell simulation on Graphic Processing Unit. The author hopes that this study will help in the design of a compact accelerator and give a decent picture of this field for those who are interested.

1.2 Aims and Objective of the Study

1. To investigate the effects of background plasma density and magnetic field on plasma wake and energy distribution of laser-type wakefield accelerators

1.3 Significant of the Study

This research study shows the tendency of energy distribution and plasma wake in LWFAs responding to the change in plasma density

1.4 Scope of the Study

1. Study dependence of electron energy distribution on 3 parameters: chamber plasma density, laser's strength parameter and background magnetic field
2. Study dependence of plasma wake's shape on 2 parameters: chamber plasma density and laser's strength
3. Study is taken for only fully-ionized cold hydrogen plasma

CHAPTER TWO: Literature Review

In this chapter, research and theories about plasma wakefield are summarized and discussed. The topic of optimum plasma density and background magnetic field which are the main investigation of this project.

2.1 Wave-Induced acceleration

Acceleration of charge particles using the electric field generated by the wave of charge density is called plasma acceleration, which is the same thing to plasma wakefield acceleration. In this project, I usually use the term “wakefield acceleration” since it provides more concrete image of the acceleration process via wakefield.

Anyway, the system of plasma wakefield acceleration is not the sole system that exhibits wave-induced acceleration. Such an acceleration can be observed in one popular sport, surfing. Surfers use surfboard to keep themselves on the surfaces of water waves as they propagate. The water interacts with surfboard and results in the force pushing the board and corresponding surfer along the direction of wave propagation.



Fig. 2.1 Surfing sport

source: <https://www.surfertoday.com/images/stories/surfingsport.jpg>

In this system, the water waves do provide acceleration to the surfboards and their surfers. The simplified version of the system of surfing can be achieved by implementing a constraint that surfers are to move horizontally only in the direction of wave propagation and are bounded to water surface. The picture on simplified surfer system can be illustrated as Fig. 2.2.

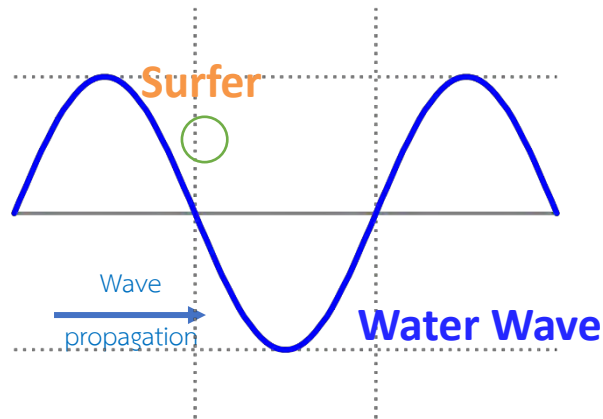


Fig 2.2 Simplified picture of wave surfing

In this model, the surfer's real velocity plays important factor. If the surfer is too fast comparing to the wave propagation, then the surfer will eventually go the back side of front peak that will decelerate the surfer. On the other hand, if the surfer velocity in the wave propagation direction is too low, the surfer will fall behind the peak and result in termination of acceleration process. Another important case is for the surfers with velocity close to the velocity of wave propagation. The surfers will be bounded between two peaks of water wave and travel along one another. This condition can be regarded as the surfers are trapped in the water wave.

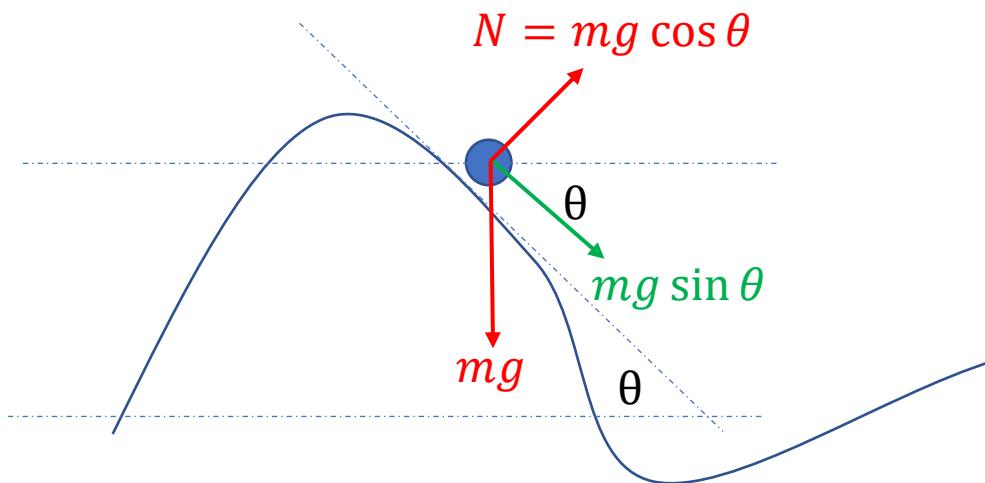


Fig 2.3 Force diagram of surfer model

The surfer motion in previous paragraph is one of existing system that provide acceleration on particle by wave. However, I found that reconstruct the phenomenon in mathematical expression can be achieved by simple toy model. Before we present the idea of toy model, another important characteristic of the surfer motion should be mentioned. For the surfer to be on the water surface all the time, the corresponding normal force from water, acting on surfboard, is equal to $mg \cos \theta$ which cancel out the

gravitational force on surfer in normal direction. The resultant force from normal force and gravitational force on surfer is $mg \sin \theta$ directs along the surface.

The diagram of surfer system is illustrated in Fig. 2.3. The surfer is shown as the blue circle on the wave profile. The actual forces acting upon the surfer, which are water – normal force and weight of surfer, are shown in red color while the resultant force is shown in green. The angle can be expressed as derivative

$$\tan \theta = -dy/dx.$$

Consider the shallow sinusoidal wave which

$$y(x, t) = \varepsilon \sin(kx - \omega t)$$

where $|\varepsilon k| \ll 1$. In this condition, the derivative dy/dx is small that the approximation

$$\theta \cong -\frac{dy}{dx} = \varepsilon k \cos(kx - \omega t)$$

is valid. In this case, the resultant force in horizontal direction is

$$mg \sin \theta \cos \theta \cong mg\theta = mg\varepsilon k \cos(kx - \omega t),$$

states that the force from shallow wave acting upon the surfer is in form of sinusoidal wave. From the shallow wave surfer system mentioned, we can reconstruct the simple equation of motion and investigate the wave-induced acceleration of simple toy model in section 2.2

2.2 Toy model of wave-induced acceleration

Consider the motion for particle of mass m subjected to the sinusoidal wave of force in 1 dimensional space,

$$F = F_0 \cos(kx - \omega t)$$

The equation of motion for the particle is

$$\ddot{x} = \frac{F_0}{m} \cos(kx - \omega t).$$

The equation of motion can be solved exactly, and the particle position as function of time can be written in linear combination of linear term and a special function called Jacobi Amplitude function $\text{am}(x, \theta)$.

$$x(t) = \frac{\pi}{2} + \frac{\omega t}{k} + \frac{2}{k} \text{am} \left(\frac{1}{2} \left(\sqrt{\frac{2F}{m} c_1 k^3 + \frac{2F}{m} k + \omega^2} \right) (c_2 \pm t), \frac{\frac{4kF}{m}}{\frac{2F}{m} c_1 k^3 + \frac{2F}{m} k + \omega^2} \right)$$

The first term $(\frac{\pi}{2} + \omega t)/k$ is linear in time of motion where $\frac{\omega}{k}$ in this context is the propagation speed of sinusoidal force wave upon the particle. The second term is Jacobi amplitude function which is the function of two arguments. In this model, the second argument is constant while the first argument is linear in time. Therefore, the second argument determines the behavior of function over time.

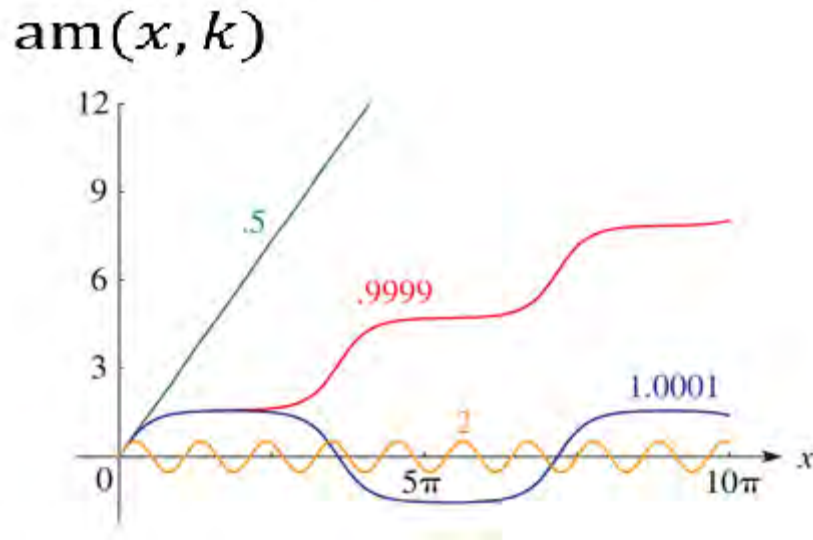


Fig 2.4 Jacobi amplitude function

Fig. 2.4 shows the behavior of Jacobi amplitude function, the numerical label for each graph denotes the value of second argument of function. The characteristic of function if this function is different for 2 regions, $|\theta| > 1$ and $|\theta| < 1$. If $|\theta| > 1$, the Jacobi amplitude function oscillates as the first argument varies. Meanwhile, the Jacobi amplitude function is monotonic (increase or decrease) function in the other region. Since the position of particle in our toy model is linear combination of linear term and Jacobi amplitude function, long time behavior of particle position is linear manner whether the Jacobi amplitude function is monotonic or oscillating function.

From the solution of equation of motion, wave-induced acceleration can be found. A particle at rest at the initial time is likely to move away from the initial position as the position changes in linear manner over long time. Therefore, the particle's average velocity will not be zero and hence, the acceleration occurs.

2.3 Plasma Wakefield Accelerator and Laser Plasma Wakefield Accelerator

Since we have investigated the toy model of wave-induced acceleration and found that oscillating force wave acting upon a particle can result in particle acceleration along the direction of wave propagation. The next step is to adapt the idea for construction of particle accelerator. The conventional particle accelerators utilize the electromagnetic field to accelerate a beam of charged particle into higher energy and confine them into a definite beam. The type of wave that can directly accelerate charged particles is electromagnetic wave like conventional accelerators. However, the other types of wave that can indirectly accelerate charge particles is charge density wave. Charged particles inside the charge density wave are influenced by electric field generated by gradient of charge density wave. Therefore, the charge density wave should be a suitable candidate for wave-induced acceleration of charged particle. The remaining question is how we practically prepare such charge density waves for actual implementation.

In order to find the method to create density wave that can accelerate charge particles, we have to consider the most frequently observed type of wave called wake. Wake is the type of wave that can be seen in daily basis. The wave generated along the path travelled by a boat in river is called wake and it is first investigated by lord Kelvin who successfully predict the feather-like pattern of water surface wake.



Fig 2.5 Water wake

source: <https://en.wikipedia.org/wiki/Wake>

However, the term “wake” is also used in plasma wakefield acceleration and it is understood for the wave that is generated by moving perturbative agent. The boat on water surface continuously cause the surface perturbation and result in wake wave behind the boat. Generation of wake in plasma can result in charge particle density. Nevertheless, the moving perturbative agent injected into plasma volume is the main factor to determine the characteristic of plasma wake. The first type of perturbative agent used in actual experiment is high-energy proton bunch in AWAKE experimental section in CERN. The proton bunch repels plasma’s ions and attracts electrons, result in blowout of and high-density electrons ions near the

proton bunch. Charge density near the proton bunch due to plasma's particles is then highly negative. The plasma ions are attracted by negative space charge at the site of bunch while electrons repel one another, resulting in electron blowout and high positive charge density at a site. The blowout electrons are then attracted back, and the ions repel on another. The processes are repeated after the bunch pass and result in long charge density wave behind proton leading bunch. The type of wakefield accelerator that use a bunch of charge particle as perturbative agent is called plasma wakefield accelerator (PWFA). Another type of perturbative agent used in actual wakefield experiment is laser. This type of accelerator is called laser-plasma wakefield accelerator (LWFA). The nature of perturbation in plasma particle by laser is vastly different from the phenomenon in PWFA. Laser provides oscillating electric field which make the electrons and ions inside plasma volume oscillate. If the laser's electric field have the same magnitude over a specific range of laser profile, then electrons and ions will oscillate about their initial positions. In order to generate the charge density wave, the laser electric field's magnitude should not be the same for all the region. This claim is based on the force called ponderomotive force which is the force acting on all charge particle moving inside the oscillating electromagnetic field of non-constant magnitude. The ponderomotive force is given by

$$\mathbf{F}_p \equiv -\frac{m_e^2 q^2}{m_q e^2} c^2 \nabla \left(\frac{a^2}{2} \right),$$

where \mathbf{F}_p denotes the ponderomotive force, m_q is for charge particle's mass, c is for the light speed in vacuum, q is charge of particle, and \mathbf{a} is normalized vector potential defined as

$$\mathbf{a} = \frac{e\mathbf{A}}{m_e c^2}$$

which is $e\mathbf{A}$ can be regarded as some quantity that define particle energy for particle of charge e and is normalized by the rest mass energy of electron. Ponderomotive force can be easily obtained by successive approximation of charged particle fluid. Consider electron's non-relativistic motion in oscillating electric field, satisfying Lorentz equation

$$\frac{D\mathbf{p}}{dt} = q \left[\mathbf{E} + \frac{\mathbf{v} \times \mathbf{B}}{c} \right]$$

where relativistic version of the equation uses the relativistic momentum instead and D denotes material derivative. The laser's electromagnetic field can be described by vector potential as

$$\mathbf{E} = -\frac{\partial \mathbf{A}}{\partial(ct)}, \quad \mathbf{B} = \nabla \times \mathbf{A}$$

Define quiver momentum

$$\mathbf{p}_q = \frac{eA}{c} = m_e c \mathbf{a}.$$

Then the time derivative can be calculated

$$\partial \mathbf{p}_q / \partial t = -e\mathbf{E}$$

Define the real momentum of charge particle fluid as linear combination of quiver momentum and correction term $\mathbf{p} = \mathbf{p}_q + \delta\mathbf{p}$. Keep only the second order terms of derivative, the equation of motion becomes

$$\frac{D\delta\mathbf{p}}{dt} \cong -m_e c^2 \nabla(a^2/2).$$

From the governing equation of fluid, the right-handed side describes the force. Since the quiver momentum oscillates, therefore, the electrons motion is bounded around their initial positions. Then the collection term $\delta\mathbf{p}$ is only term to determine the averaged motion of electrons. In large time scale, the average motion due to quiver momentum vanishes, then the motion can be seen as the particle subjected to ponderomotive force alone. The characteristics of ponderomotive force are following:

- Ponderomotive force acts on all non-neutral particle in the same manner
- It points toward the region where laser's field is weaker
- For a given laser pulse, ponderomotive force magnitude on a charged particle is inverse proportion to the charge's mass

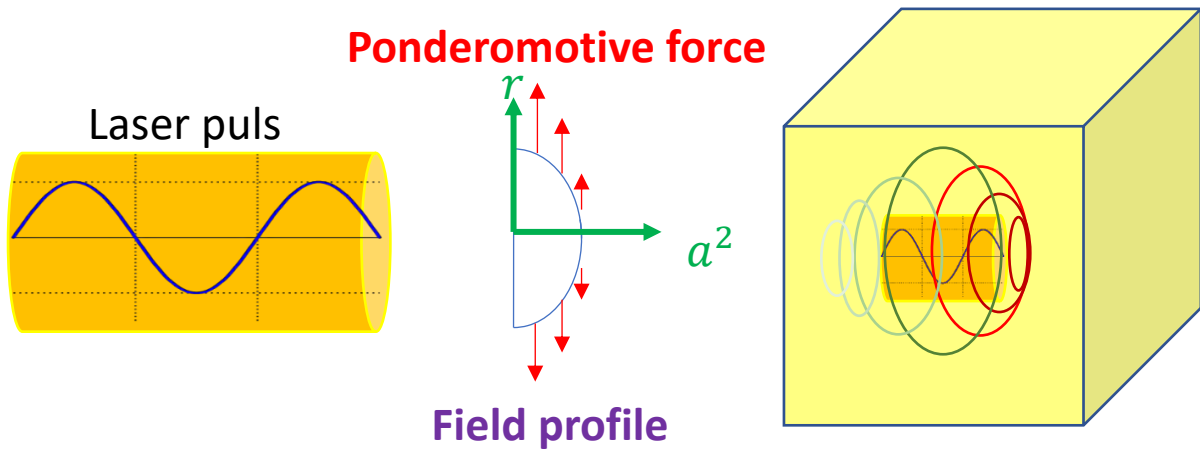


Fig 2.6 Ponderomotive force diagram

From those characteristics, when a laser pulse propagates through a plasma volume, plasma particles are dispersed from the laser toward weaker field region. The dispersion generated by the ponderomotive force then generates the space charge and its electric field. The space-charge then attracts or repels other plasma particles in the same manner of plasma wakefield accelerator with leading proton

bunch considered above, and results charge density wave that can be used to accelerate charged particles. However, another consequence from ponderomotive force's characteristic is that electrons and ions do not experience the same magnitude of repulsion force from the laser. Without considering relativistic effect, in case of proton, whose mass is approximately 1800 times of electron mass, the ponderomotive force is 0.056% of the ponderomotive force experiencing by electrons. Taking the mass into account, the acceleration of protons is about $(1/1800)^2$ times of the acceleration of electrons. The difference is lower for relativistic case since electrons are more influenced by ponderomotive force. Electrons are likely to move with higher speed compare to ions and the ratio m_e/m_i increase by γ factor. Therefore, in usual case, ions are considered motionless and only electrons are responsible for variation in charge density wave.

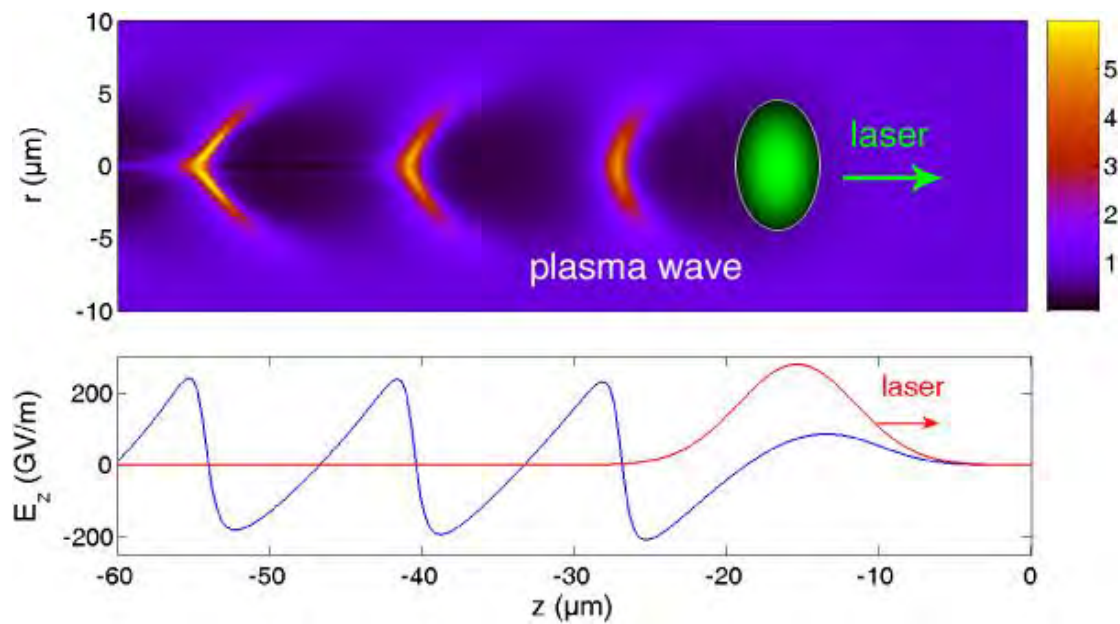


Fig 2.7 Plasma wake and plasma wakefield

source: <https://cds.cern.ch/record/2203628/plots>

From the Fig. 2.7 electrons are repelled from the laser pulse as the results of ponderomotive force. The chain of ions bubbles is observed in Fig. 2.7. Electron's cross-sectional density plot shows the region of low electron density behind the laser pulse while electron peaks occurs between the ion bubbles. The ion bubbles and electron peaks form the electron density wave which can be used to accelerate charge particles.

The idea of wakefield accelerator first comes in the form of laser-plasma wakefield by Tajima (6). The lead in LWFA is laser whose traveling speed in plasma is $(1 - \omega_p^2/\omega^2)c$ where ω_p, ω, c denotes plasma frequency, laser frequency, and speed of light respectively. If charge particles are trapped between the wakes propagating with the same speed, their relativistic kinetic energy is then γmc^2 where γ is Lorentz factor value $(1 - \omega_p^2/\omega^2)^{-1/2}$. Thus, if charge particles pick up their speed from rest, the minimum energy

gain will be $\left[(1 - \omega_p^2/\omega^2)^{-\frac{1}{2}} - 1 \right] mc^2$. However, if the lead in wakefield accelerator is particle bunch, the phase velocity of wave can be made arbitrary close to the speed of light (this of course, would require acceleration). The particle being used should interact with plasma in the way that generate large perturbation in positions along its course of propagation. The particles in question are charge particle. Charge particles not only interact with other particles through collisions, but also far-apart charge particles via Coulomb force (although in plasma the effects are screened out by shielding) to create a larger space charge for wake. If we use the electrons as drivers (another name for lead), their small mass will cause a fast wave degrading. AWAKE experiment by CERN uses other charge particle with the same magnitude of charge, proton, as driver lead. Since a proton is about a thousand times larger than an electron in mass, the problem of lead degrading is lessened. One advantage of using proton driving bunch is availability of high-energy protons beam since high-energy proton are already used in CERN's Super Proton Synchrotron (SPS). Another important trait to mention for CERN's AWAKE is from Seed-Self Modulation (SSM) of proton bunch propagating in plasma. SSM process divides a long bunch of protons into a short bunch of plasma wavelength that can drive wakefield resonantly.

2.4 Enhancing wakefield accelerator

Many modifications are made in wakefield accelerator to exceed the energy gain limit, ω_p^2/ω^2 , proposed by Tajima in his publication (6). One of those methods is using two laser-lead pulses with beat frequency matching plasma frequencies; it enhances the maximum gain to $2\omega_p^2/\omega^2$ (7). Another modification made is utilization of static magnetic field in direction of wakefield propagation. This idea was formulated by T. Katsoulas and Dawson, using the fact that magnetic field perpendicular to electrons motion causes circulation of electrons. The appropriate magnitude of magnetic field will keep electron in phase with the wake and gain more energy. However, the electromagnetic wave in previous situation requires long plane EM wave and the accelerated electrons also move perpendicular to wave with speed comparable to the speed of light. Long-plane EM waves are hard to achieve, also the two-dimensional motion generated by presence of magnetic field requires larger volume of plasma in accelerator. There is another study of magnetic field in wakefield accelerator taken in 2008 (8), in which the magnetic field pointed along the direction of laser propagation. Results were that longitudinal magnetic field application enhances particle energy gain and also trapping. This way of magnetic field application does not require larger cross section of accelerator, then the particle mostly move in the same direction, hence, be more appropriate for generation of beam. The other way for enhancing wakefield accelerator is to making lead modification. Like beat-wave wakefield accelerator, the lead of appropriate shape and density (or intensity) can enhance acceleration in wakefield accelerator. Since acceleration depends on lead density, it may, as well, depends on plasma density in chamber. Recent research on nonlinear theory of plasma wakefield suggests that the electric field inside wakes of wakefield accelerator depends on both background plasma

density and density of lead electrons. The maximum acceleration gradient in blowout regime are achieved if the density values are approximately the same. However, blow out mechanisms are different from particle lead type. Therefore, there is no parametrization for particle lead density and laser amplitude in theory. Optimum lead value of each type is determined separately. Unlike lead type, plasma density plays the same role for both types of wakefield accelerator, and plasma density optimization is applicable for all type of wakefield accelerator. Normally, leading bunches are not easily changeable, then plasma density optimization is more practical than variation of lead power. In famous particle-lead experiment, CERN's AWAKE, proton lead bunches are remnant from Synchrotron section. Meanwhile, in LWFA, laser powers are mostly limited by the generator. Reshaping the pulse requires complicate design of tools (9) (10). In order to realize laser shaping, simulations are used for apparatus design as well. So, LWFA studies for optimum lead are mostly done through simulations.

2.5 Enhancing wakefield accelerator by longitudinal magnetic field

In LWFA, additional field can be applied to enhance acceleration ability. Both electric field and magnetic field affect particle motion inside the accelerator. Therefore, one method to enhance wakefield accelerator is using appropriate field. Research (8) shows that application of magnetic field in the direction of laser propagation increases the number of accelerated electrons and their resulting energy. In magnetic field, electron's blowouts are suppressed by cyclotron motion which resulting in increasing number of trapped electrons. Simple argument can be made to shows magnetic field role in electron trapping. First, determine the balancing radii force in case of no magnetic field. At the beginning of acceleration, there are no trapped electrons inside the wake. The ponderomotive repelling force is equal to attraction from space charge or bubble. As time passes, some electrons come inside the wake, and are trapped. Trapped electrons deliver repelling force to other electrons at the edge of blow due to coulomb force. Introducing magnetic field increase attraction force in radii direction and reduce effect of coulomb repelling force from trapped electrons. Therefore, more electrons can be trapped inside the wake. However, excessive value of magnetic field will suppress electron's blowout and the generation of wake. The effects of magnetic field to wakefield accelerator are thoroughly investigated in (8).

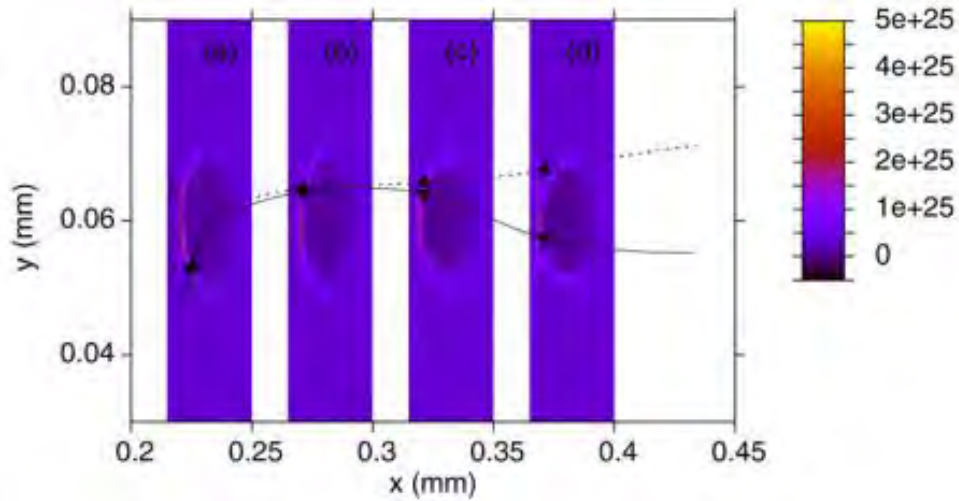


Fig 2.8 Transverse motion suppression in LWFA with axial magnetic field

Fig 2.8 shows the track of one electron inside laser-plasma wakefield accelerator in two case: with axial magnetic field and without axial magnetic field. To investigate the cause of increase in number of trapped electrons, probe particles with the mass and charge of electron are traced. The trajectory of probe particle inside LWFA without magnetic field is traced by dash curve. On the other hand, the solid curve shows the trajectory for LWFA with axial magnetic field of magnitude 120 Tesla. From the trajectories of probe particle, it is obvious that axial magnetic field inhibits the transverse motion of probe particle which is why number of trapped particle increase.

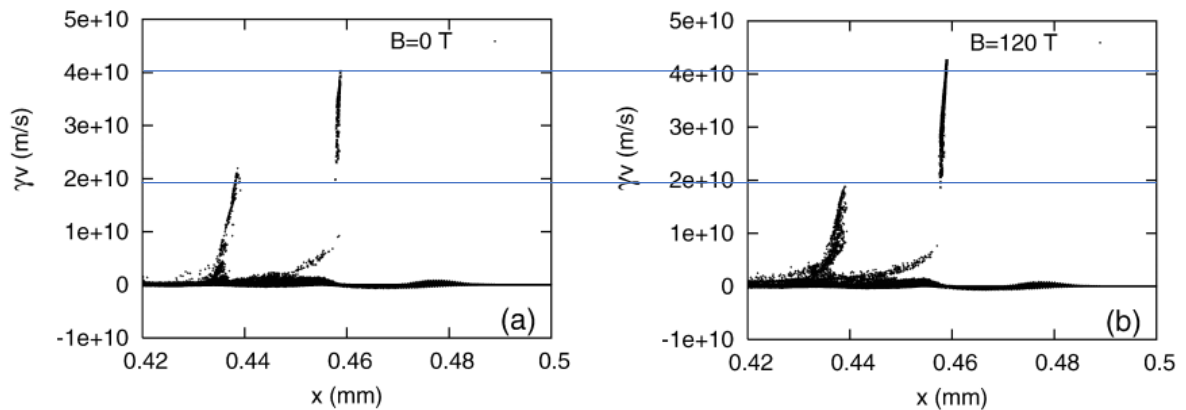


Fig 2.9 Electron beam's energy enhancement by axial magnetic field

Another effect of axial magnetic field is energy enhancement of accelerated beam of electrons. The phase space of electrons shows that electrons inside LWFA with axial magnetic field of 120 T achieve higher maximum momentum compare to LWFA without background magnetic field. However, the enhancement observed in this result occurs only for the electrons that are trapped in the frontmost ion bubble, the first bubble. In contrast, electrons inside the acceleration field of the second bubble have lower maximum

momentum for LWFA with axial magnetic field of 120 T. This research (8) focuses more on the enhancement on the first bubble and the range of magnetic field magnitude considered is small, therefore this matter of magnetic field effect in LWFA should be investigated more.

2.6 Plasma density effects on wakefield accelerators

Value of plasma density affects wakefield accelerator in various aspects as being described in theoretical study (4). Plasma density directly affects plasma frequency which described time scale for weak oscillation of plasma density inside plasma volume. Consequently, parameters and observables relate to plasma frequency are also indirectly affected by the density. First, plasma density affects the plasma frequency which is a parameter describing time scale of small oscillation inside plasma volume. Second thing related to plasma density is blowout radius of wake. In plasma wakefield accelerator with particle lead, the blowout of electrons is due to coulomb force. The blowout radius can be approximated by balancing repelling force from leading bunch with attraction from positive space charge. However, it is different for laser wakefield accelerator. Laser bunch, unlike charge particle, cannot assert electric field and force upon particles outside the bunch range. Moreover, electrons in laser wakefield accelerator are not only repelled out but also attracted by laser's field as well. Blowout of electrons, in this case, are caused by uneven maximum laser's field. The electrons at the front of laser bunches are oscillated by laser's field, first order motion of those electrons is oscillation with the frequency of laser. This first order motion is not enough to describe blowing out of electrons. The smooth expelling force called ponderomotive force can be explained as second order motion of charge particle at laser front. Therefore, second order motion is enough for considering electrons inside wakefield accelerator. Typically, ponderomotive force acts on all charged particles. However, the magnitude of ponderomotive force is $\mathbf{F}_p = -\frac{q^2}{4m\omega^2} \nabla(E^2)$ which is inversely proportional to the mass of the corresponding charge. Therefore, the force acts upon proton is approximately thousand times smaller than that upon electrons. Moreover, accounting for the ratio of mass, protons' motion is approximately million times slower than electrons interacting with the same laser pulse. Then, for some range of laser magnitude, protons are approximately motionless, and dynamics of system is completely determined by electrons behavior. Blowout radius of laser-type wakefield accelerator can be approximated by equating outward ponderomotive force and inward space charge attraction force. Since the inward attraction from positive space charge is proportional to protons density composite of that space charge, plasma density also has influence on this parameter. The third parameter being affected by plasma density is laser's group velocity. Since laser is electromagnetic wave, it propagates in vacuum with light speed and in other medium, laser propagates with a group velocity slower than its vacuum speed. In wakefield accelerator, laser propagate with the group speed slightly less than vacuum speed. Group speed of weak laser inside volume of plasma is $v_g = \left(1 - \left(\frac{\omega_p}{\omega}\right)^2\right) c$, depending on plasma density and

laser frequency. This expression of group speed is not defined for plasma frequency more than laser frequency, $\omega_p > \omega$, indicating unexplored linear region for plasma wakefield accelerator. The fourth parameter affected by density is closely related to laser group velocity. It is called dephasing length L_{dp} . Dephasing length represents the total distance inside the accelerator in which the accelerated electrons begin moving faster than the laser front. At first, electrons are trapped inside the wake's space charge, and being accelerated by space charge electric field. Gradually, electrons gain kinetic energy and their speed increases. Since electrons' speed are not bounded by laser's group velocity, eventually accelerated electrons' speed will exceed the wave front's speed and, therefore, surpass the wake's acceleration field. The electrons in this case, will be not in the region of acceleration phase by wake, thus the name "dephasing". Lastly, phenomenon related to plasma density is laser depletion. Laser propagating through plasma volume depletes over propagation distance. The higher density plasma inside accelerator means more depletion rate. The length that laser decreases its amplitude to $1/e$ is called pump depletion length L_{pd} . This depletion is to be expected from energy conservation, that is, field energy is being transferred to charge particles inside plasma chamber. After laser pulse loses its energy, the repelling force becomes weaker and results in smaller plasma blowout. Moreover, acceleration field from space charge becomes smaller too. Dephasing and pump depletion are the main limiting factor of wakefield accelerators. Unlike conventional electromagnetic accelerators, enhancing acceleration powered by increase of accelerator's length is prohibited by these factors. Dephasing limits and depletion can be solved by some additional configuration such as lead pulse modulation, or multiple-stage acceleration (11).

To summarize, plasma density affects the wakefield accelerators in at least five aspects. The density affects plasma frequency, blowout radius, laser's group velocity, dephasing and pump depletion. However, in our study, only blowout radius, pump depletion and electron acceleration are observed. The details about each topic is explained in the following paragraph.

2.5.1. Plasma frequency

Plasma is an ionized gas with high ionization ratio. Inside volume of plasma, protons and electrons are not bounded together, so that they are called free electrons (or protons). Neutral atoms typically present inside plasma as well, but they, normally, are neglected in considering of wakefield acceleration. Since protons are approximately thousand times heavier than electrons, electrons are considered more responsive compare to protons. The phenomenon inside plasma volume mostly comes from electron's behaviors.

2.5.2. Blowout Radius

Plasma density affects greatly on the shape of plasma wake. For a bi-gaussian laser pulse, electric field decreases perpendicularly to propagation. Ponderomotive force depends on the gradient of squared magnitude of electric field, and its maximum value occurs at the

distance of $\frac{\sigma_r}{\sqrt{2}}$ where, σ_r denotes standard deviation parameter for bi-gaussian shape in perpendicular direction.

2.5.3. Laser's group velocity and dephasing

In plasma wakefield accelerator, laser propagates in plasma with the magnitude of group velocity of light in plasma which is slightly lower than speed of light. However, for a particle, the maximum speed is equal to the speed of light. Therefore, particles inside constant acceleration will eventually have speed exceeding the wake propagation speed, then the particle will go out of acceleration region of wakefield and acceleration is halted. The length scale of dephasing is also proportion to ω_p^{-3} , therefore, decreases as plasma density increases.

2.5.4. Pump Depletion

Plasma wakefield accelerator utilizes laser pulse propagating through the plasma volume to create positive space charge. Typically, laser pulse depletes over distances in plasma volume. Depletion gradually lessens laser's repelling force upon plasma's charge particles, resulting in smaller positive space charge and lesser acceleration power. The depletion caused by laser interaction with charge particles and losing their energy. This phenomenon is similar to energy depletion in bullet going through a solid. High energy bullet gradually loses its energy and becomes stuck in the middle of the solid. Total distance for bullet in solid depends on solid's density, lower density lessens energy depletion rates and results in longer total bullet's distance in solid. In plasma wakefield accelerator, the depletion length scales are proportional to the factor $(\omega/\omega_p)^2$, where ω and ω_p denote laser's angular frequency and plasma frequency respectively. Since $\omega_p = (ne^2/m^*\epsilon_0)^{1/2}$ in SI unit, depletion length scales are then inversely proportional to plasma density.

2.5.5. Electron Acceleration

Plasma density also affects the electric field created inside the wake. Since the acceleration field is electric field created by positive space charge caused by blowing out of plasma by laser's ponderomotive force. However, ponderomotive force is inversely proportional to mass of charge particles, therefore only electrons with small mass compare to protons are blown out. For plasma, which consists of even distribution of electrons and protons, the electric field is zero. Therefore, acceleration field is equal to electric field from only space charges. Therefore, electric field depends highly on plasma density and the shape of positive space charge. If electrons are completely blown out,

the electric field inside wakefield is proportion to plasma density and corresponding shape. If laser power is not strong enough for the electrons to be not completely blown out, then the acceleration electric field is lower. Plasma density also affects the acceleration of wakefield accelerator. The example can be found in complete blowout case. In this case, electrons are repelled out to the edge of the wake. At the edge, zero net force acts on the electrons in radial direction. The repelling force from laser and attraction from space charge are equal in this direction. Since, attraction force depends on plasma density, the blowout radius depends on plasma density as well. Higher plasma density means higher attraction force, and so lower blowout radius. Excessive density value makes space charge insufficiently small to produce high acceleration gradient. In this project, electron acceleration is probed by energy histogram.

2.7 Particle-in-Cell method

Particle-in-cell method is a technique used in solving PDEs of certain classes. After suggestion of Dawson *et al.* in his publication “Particle simulation in plasma” (12), where he treated the problem of many finite-volume body with coulomb interaction. His method is accepted and became conventional method for plasma simulation. PIC method usually follows these steps:

1. Particles’ positions and velocities are collected.
2. Moments of distribution such as charge densities, currents are assigned to fixed mesh points.
3. The field and force of interaction on exact positions of each particle are calculated from the moment distributions on mesh point.
4. Equation of motion is discretized and used to update the moment distribution in the next time step.
5. Repeat the procedures.

Since the calculation is taken by the operation’s number proportion to number of particles in the system, an additional procedure of super-particle can be made to alleviate required computational resource. Super-particles are groups of many particles bunched together. Particles in the same bunch do not interact with others. The additional modification can be made in various part of PIC method such as particle mover (or pusher), field solver, and particle/field weighting.

Particle mover is a tool used for making an update in particles’ position and velocity. It requires the most computational time in all PIC component because the processes of mover must be done for each particle separately.

The field solver used in PIC simulation of plasma to solve Maxwell’s equation. The most common methods used are Finite-Element, Finite-Difference and spectral method.

CHAPTER THREE: Research Methodology

In this chapter, the research design and method for data analysis are explained in detail. Research design includes all ordered processes required from the beginning throughout the entire work. Next, schedule for each process is shown. Finally, the method for data analysis is described and discussed for its limitation.

3.1 Research Design

1. Study of basic plasma physics and literature review of wakefield accelerator

The study of basic plasma physics involving plasma skin depth, collective behavior, fluid model, plasma oscillation, dynamics of plasma.

2. PIConGPU documentation review

a. Dimensional of simulation

Expectations: Be able to adjust the simulation's dimension

b. Laser lead configuration

Expectations: Be able to adjust the intensity of laser field and pulse shape of laser

c. Background field configuration

Expectations: Be able to assign a desired background field (both \vec{E} and \vec{B}) onto our wakefield system

3. Chalawan's cluster

Submit the proposal to NARIT's Chalawan management team and gain the access to Chalawan's pollux site which controls GPU nodes. The GPUs accessibility granted are needed in order to realize PIConGPU simulations.

Expectations: Grant permission to access NARIT's Chalawan

4. Simulation setup of PIConGPU on Chalawan

Set up an environment for PIConGPU simulation inside NARIT's Chalawan.

Expectations: Adjustable PIConGPU simulation on Chalawan's Cluster

5. Density effect on wakefield accelerator

Observe and collect data of energy distribution and for a fixed laser strength.

Expectations: Graph that illustrates the relation of responses to background plasma density at various conditions

6. Density and lead amplitude relevant investigation

Study effects of background plasma density with laser strength on energy distribution of LWFAs.

Expectations: Graph that illustrates the relation of responses to background plasma density at varying lead amplitude values

7. Magnetic field effects

Study effects of background plasma density with lead plasma density (or laser intensity) on electron trapping of wakefield accelerators. The study is taken with the same configuration of the step 6.

Expectations: Graphs that illustrate the relation of responses to background magnetic field of different values are shown and compared to results in step 6.

8. Analysis and summarize

Analyze information obtained in step 5-8 and compare with reviewed articles then determine this project hypothesis with data from step 9. Data is visualized to informative graph or picture and put together in summary.

9. Report writing

10. Final presentation and discussion

3.2 Gantt chart

No	Step	Sep /19	Oct /19	Nov /19	Dec /19	Jan /20	Feb /20	Mar /20	Apr /20	May /20
1	Study of basic plasma physics and literature review of wakefield accelerator	/	/	/						
2	PICongPU documentations review	/	/	/						
3	Chalawan's cluster permission		/							
4	Output processing program		/	/	/	/	/			
5	Simulation setup of PICongPU on Chalawan			/						
6	Density effect on wakefield accelerator			/	/					
7	Density and lead amplitude relevant investigation				/	/				
8	Magnetic field effects					/	/			
9	Analysis and summarize			/	/	/	/			
10	Report writing			/	/	/	/	/		
11	Final presentation and discussion								/	/

CHAPTER FOUR: PIConGPU

4.1 Overview

PIConGPU is abbreviated from Particle-In-Cell on Graphic Processing Unit. It is a package on Linux operating system imbued with NVIDIA's GPUs with ability to simulate a fully relativistic plasma PIC algorithms. Moreover, it supports a hybrid architecture consists of one computational node interconnected with a standard cluster topology which node carry one or more GPUs. PIConGPU is also the first scalable GPU cluster implementation of PIC.

PIConGPU package consists of several selectable numerical schemes to solve PIC cycle. We can choose a set of numerical method appropriate to simulate the system of interest. However, using highly efficient method require more computational resources which are limited in this project. To simulate LWFA on NARIT's CHALAWAN, we are required to use lower efficiency numerical method to be able to initiate simulation. This matter regarding simulation setup will be further clarified in section 4.3.

4.2 Parameter file

PIConGPU is a package of text file for further compilation into an executable simulation program. The users are required to input the information such as numerical method, memory allocation, simulation size and initial configuration that will be used in the simulation to compilation system. After input file are ready, users use the command `pic-buid` to compile and build an executable file for the simulation. After the building processes are completed, the users either run the simulation file by themselves or submit the job to their corresponding administration system using built-in command `tbg`. The parameter file in PIConGPU package are labelled by `.param`. Important parameter files in this project are following:

4.2.1 density.param

Describes the initial plasma particle distribution over the simulation space. The first part of `density.param` is about defining parameter `BASE_DENSITY_SI` in unit of m^{-3} .

```
/** Base density in particles per m^3 in the density profiles.
 *
 * This is often taken as reference maximum density in normalized profiles.
 * Individual particle species can define a `densityRatio` flag relative
 * to this value.
 *
 * unit: ELEMENTS/m^3
 */
#ifndef PARAM_BASE_DENSITY_SI
#  define PARAM_BASE_DENSITY_SI 7.0e24
#endif
constexpr float_64 BASE_DENSITY_SI = PARAM_BASE_DENSITY_SI;
```

Fig 4.1 Base density definition in density.param

In this example, the parameter `PARAM_BASE_DENSITY_SI`'s default value is $7.0 \times 10^{24} \text{ m}^{-3}$. At the end of this section, the parameter `BASE_DENSITY_SI` is assigned with the value of `PARAM_BASE_DENSITY_SI`.

```

PMACC_STRUCT(GaussianParameter,
    /** Profile Formula:
    *   constexpr float_X exponent = abs((y - gasCenter_SI) / gasSigma_SI);
    *   constexpr float_X density = exp(gasFactor * pow(exponent, gasPower));
    *
    *   takes `gasCenterLeft_SI    for y < gasCenterLeft_SI`,
    *         `gasCenterRight_SI   for y > gasCenterRight_SI`,
    *   and exponent = 0.0 for gasCenterLeft_SI < y < gasCenterRight_SI
    */
    (PMACC_C_VALUE(float_X, gasFactor, -1.0))
    (PMACC_C_VALUE(float_X, gasPower, 4.0))

    /** height of vacuum area on top border
    *
    *   this vacuum is important because of the laser initialization,
    *   which is done in the first cells of the simulation and
    *   assumes a charge-free volume
    *   unit: cells
    */
    (PMACC_C_VALUE(uint32_t, vacuumCellsY, 50))

    /** The central position of the gas distribution
    *   unit: meter
    */
    (PMACC_C_VALUE(float_64, gasCenterLeft_SI, 8.0e-5))
    (PMACC_C_VALUE(float_64, gasCenterRight_SI, 3.0e-4))

    /** the distance from gasCenter_SI until the gas density decreases to its 1/e-th part
    *   unit: meter
    */
    (PMACC_C_VALUE(float_64, gasSigmaLeft_SI, 8.0e-5))
    (PMACC_C_VALUE(float_64, gasSigmaRight_SI, 8.0e-5))
); /** struct GaussianParam */

/** definition of density with Gaussian profile */
using Gaussian = GaussianImpl< GaussianParameter >;

```

Profile formula for Gaussian profile

Define Gaussian parameter

Vacuum space at border

Profile parameter

Implement Gaussian profile with defined parameter using Gaussian = GaussianImpl< GaussianParameter >;

Fig 4.2 Plasma density profile in density.param

The second part of density.param is density profiling part. In this example, the profile of density is Gaussian distribution over y axis in simulation space. The description of the profile and its parameters are given in Fig. 4.2.

4.2.2 grid.param

Determine the grid separation for interpolation of field quantities such as electric field and magnetic field. This parameter file also defines the time step separation for each PIC cycle.

```
                                Timestep separation
/** Duration of one timestep
 * unit: seconds */
constexpr float_64 DELTA_T_SI = 1.39e-16;

                                Grid separation
/** equals X
 * unit: meter */
constexpr float_64 CELL_WIDTH_SI = 0.1772e-6;
/** equals Y - the laser & moving window propagation direction
 * unit: meter */
constexpr float_64 CELL_HEIGHT_SI = 0.4430e-7;
/** equals Z
 * unit: meter */
constexpr float_64 CELL_DEPTH_SI = CELL_WIDTH_SI;
```

Fig 4.3 The grid separation part of grid.param

The example in Fig. 4.3 shows some of quantities defined inside `grid.param` file. The grid separations in this case are 1.772×10^{-7} m in x and z direction while grid separation in y direction is 4.4430×10^{-8} m. Moreover, the timestep separation for each PIC cycle is 1.39×10^{-16} s.

4.2.3 laser.param

At the beginning of file, three parameters are defined. `PARAM_A0` is dimensionless quantity called normalized laser's strength parameter. Its definition is the magnitude of normalized vector potential defined in section 2.4. `PARAM_WAVE_LENGTH_SI` is the wavelength of laser in SI unit. Finally, `PARAM_PULSE_LENGTH_SI` is the vacuum length of laser pulse in SI unit. The example is shown in Fig. 4.4.

```
                                Normalized laser's strength
#ifndef PARAM_A0
#   define PARAM_A0 8.0
#endif

                                Wavelength 800nm
#ifndef PARAM_WAVE_LENGTH_SI
#   define PARAM_WAVE_LENGTH_SI 0.8e-6
#endif

                                Pulse length 5 fm
#ifndef PARAM_PULSE_LENGTH_SI
#   define PARAM_PULSE_LENGTH_SI 5.e-15
#endif
```

Fig 4.4 Laser's parameter

The next part of this file is construction of laser profile function. This part of profile construction is very complicate. However, various types of profile are prepared by developers for non-coding users. One of those profiles is gaussian profile in y direction.

4.2.4 fieldsolver.param

This parameter file is used for selection of the numerical scheme for interpolation of field quantities in simulation. The `fieldsolver.param` are divided into 2 parts: current interpolation and the field solver. The current interpolation uses information on particle velocity and particle charge to interpolate the vector field of current.

Option of current interpolation

```

/** Current Interpolation
 *
 * CurrentInterpolation is used to set a method performing the
 * interpolate/assign operation from the generated currents of particle
 * species to the electro-magnetic fields.
 *
 * Allowed values are:
 * - None:
 *   - default for staggered grids/Yee-scheme
 *   - updates E
 * - Binomial: 2nd order Binomial filter
 *   - smooths the current before assignment in staggered grid
 *   - updates E & breaks local charge conservation slightly
 * - NoneDS:
 *   - experimental assignment for all-centered/directional splitting
 *   - updates E & B at the same time
 */
#endif PARAM_CURRENTINTERPOLATION
# define PARAM_CURRENTINTERPOLATION None
#endif
using CurrentInterpolation = currentInterpolation::PARAM_CURRENTINTERPOLATION;

```

Define CurrentInterpolation = currentInterpolation::None

Fig 4.5 Current interpolation in fieldsolver.param

The file in this example does not previously define the parameter `PARAM_CURRENTINTERPOLATION`. Therefore, the parameter is chosen to be its default value which is None. Then the last line in this part define the main current interpolator that will be called in `speciesDefinition.param` file.

Option on field solver

```

/** FieldSolver
 *
 * Field Solver Selection:
 * - Yee< CurrentInterpolation >: standard Yee solver
 * - Lehe< CurrentInterpolation >: Num. Cherenkov free field solver in a chosen direction
 * - DirSplitting< CurrentInterpolation >: Sentoku's Directional Splitting Method
 * - None< CurrentInterpolation >: disable the vacuum update of E and B
 */

#ifdef PARAM_FIELDSOLVER
/* WARNING: if you change field solver by hand please update your CELL_WIDTH_SI
 * in 'grid.param' to fulfill the convergence condition (CFL)
 */
# define PARAM_FIELDSOLVER Yee
#endif
using Solver = maxwellSolver::PARAM_FIELDSOLVER< CurrentInterpolation >;

```

Define parameter Solver

Default value of solver

Fig 4.6 Fieldsolver method in fieldsolver.param

The second part of `fieldsolver.param` contains the information on the main field solver. In this example, the Solver is defined to be Yee solver. The actual implementation of solver is in `speciesDefinition.param` file.

4.2.5 species.param

Defines the numerical method used for plasma particle inside the simulation.

```

/*----- generic solver-----*/

/*! Particle Shape definitions -----
 * - particles::shapes::CIC : 1st order
 * - particles::shapes::TSC : 2nd order
 * - particles::shapes::PCS : 3rd order
 * - particles::shapes::P4S : 4th order
 *
 * example:          using CICShape = particles::shapes::CIC;
 */

#ifdef PARAM_PARTICLESHAPE
#define PARAM_PARTICLESHAPE TSC
#endif
using UsedParticleShape = particles::shapes::PARAM_PARTICLESHAPE;

```

Particle shape interpolation option

Using second order shape

Fig 4.7 Particle shape interpolation

In this example file, the particle shape interpolation is 2nd order particle shape as the main particle to field interpolator. Note that `species.param` only defines `UsedParticleShape`. The process of using interpolator is actually in `speciesDefinition.param`. Higher order particle shape gives more accurate numerical simulation, however it requires more memory used in calculation.

Option of numerical schemes

```

/#!/ particle pusher configuration -----
*
* Define a pusher is optional for particles
*
* - particles::pusher::Vay : better suited relativistic boris pusher
* - particles::pusher::Boris : standard boris pusher
* - particles::pusher::ReducedLandauLifshitz : 4th order RungeKutta pusher
*                                           with classical radiation reaction
*
* For diagnostics & modeling: -----
* - particles::pusher::Free : free propagation, ignore fields
*                           (= free stream model)
* - particles::pusher::Photon : propagate with c in direction of normalized mom.
* - particles::pusher::Probe : Probe particles that interpolate E & B
* For development purposes: -----
* - particles::pusher::Axel : a pusher developed at HZDR during 2011 (testing)
*/
#ifdef PARAM_PARTICLEPUSHER
#define PARAM_PARTICLEPUSHER Boris
#endif
using UsedParticlePusher = particles::pusher::PARAM_PARTICLEPUSHER;

```

Using Boris pusher

Fig 4.8 Particle pusher selection in species.param

The particle pusher algorithm which update particle's velocities and positions is determined in this parameter file as well. This part is very important as the particle pushers that can be used in relativistic region are Boris and Vay pusher. Boris pusher is good enough numerical scheme to push particle in relativistic region, however, it does not operate well in ultra-relativistic region. The better version of Boris pusher, Vay pusher is more appropriate to simulate system in ultra-relativistic region.

4.2.6 speciesDefinition.param

Define the properties of plasma particle by species. The quantities such as mass, charge and the numerical particle pusher algorithm are defined in this file.

```

/*----- ions -----*/
/* ratio relative to BASE_CHARGE and BASE_MASS */
value_identifier( float_X, MassRatioIons, 1836.152672 );
value_identifier( float_X, ChargeRatioIons, -1.0 );
using ParticleFlagsIons = MakeSeq_t<
  particlePusher< UsedParticlePusher >,
  shape< UsedParticleShape >,
  interpolation< UsedField2Particle >,
  current< UsedParticleCurrentSolver >,
  massRatio< MassRatioIons >,
  chargeRatio< ChargeRatioIons >,
  ionizers<
    MakeSeq_t<
      particles::ionization::BSIEffectiveZ< PIC_Electrons >,
      particles::ionization::ADKCircPol< PIC_Electrons >
    >,
    ionizationEnergies< ionization::energies::AU::Hydrogen_t >,
    effectiveNuclearCharge< ionization::effectiveNuclearCharge::Hydrogen_t >,
  >,
  atomicNumbers< ionization::atomicNumbers::Hydrogen_t >
>;
/* define species: ions */
using PIC_Ions = Particles<
  PMACC_CSTRING( "i" ),
  ParticleFlagsIons,
  AttributeSeqIons
>;

```

mass and charge

ionization part of Flags

Flags sequence

Species Sequencing lines

Fig 4.9 Species' attributes sequencing

Fig 4.9 shows a section which defines the properties of protons. The `value_identifier` lines defines the charge and mass of proton, relative to those of electrons. First line, `value_identifier(float_X, MassRatioIons, 1836.152672)` means that the `MassRatioIons` parameter is created with the numerical value 1836.152672 which is relative mass of proton to electron. For Helium plasma, this ratio should be 2 times higher. The last step in construction of a species is to use all defined parameter to sequences the species in using `PIC_<species name>` which species name is `Ions` in this example. The `particles` function on the right-hand side of `PIC_Ions` have 3 arguments: PMACC string, flags, and attribute sequence.

First, PMACC string is label of species for further operations. Second, Flags containing information on interpolation schemes that are used for this species for each timestep. Finally, attribute sequence is phase space of species at the initial states.

PMACC_CSTRING("i") means that from the particle is labelled as "i". In multi-species plasma, we can selectively track the behavior of particles in one species using this labelled. Since this senior project consider single-species plasma, the labelled used in simulation are "i" for protons and "e" for electrons.

ParticleFlagIons is the sequence of numerical schemes for species Ions as defined above. However, users are free to adjust the type of numerical scheme used for each species in this file. We can ignore the motion of ions by use no particle pusher for ion's species, or we can use the lower order scheme in some species that have negligible change in observation interval.

4.2.7 fieldbackground.param

Defines the background electric field and magnetic field inside the simulation. This parameter file can be divided into 3 parts: electric field, magnetic field and current density field.

```

class FieldBackgroundE
{
public:
    /* Add this additional field for pushing particles */ On/off electric field
    static constexpr bool InfluenceParticlePusher = false;

    /* We use this to calculate your SI input back to our unit system */
    PMACC_ALIGN(m_unitField, const float3_64);

    HDINLINE FieldBackgroundE( const float3_64 unitField ) : m_unitField(unitField)
    {}

    /** Specify your background field E(r,t) here
     *
     * \param cellIdx The total cell id counted from the start at t = 0
     * \param currentStep The current time step */
    HDINLINE float3_X
    operator()( const DataSpace<simDim>& cellIdx,
               const uint32_t currentStep ) const
    {
        /* example: periodicity of 20 microns ( = 2.0e-5 m) */
        constexpr float_64 period_SI(20.0e-6);
        /* calculate cells -> SI [m] */
        const float_64 y_SI = cellIdx.y() * SI::CELL_HEIGHT_SI;
        /* note: you can also transform the time step to seconds by
         * multiplying with DELTA_T_SI */ Define the argument of sinusoidal electric field

        /* specify your E-Field in V/m and convert to PICongGPU units */
        const float X sinArg = precisionCast<float X>( y_SI / period_SI * 2.0 * PI );
        return float3_X(0.0, 0.0 / m_unitField[1], 0.0); Electric field components
    }
};

```

Fig 4.10 Class of background electric field

An example of electric field part is shown in Fig. 4.10. In this case, the electric field is not included in calculation of PIC cycle because the Boolean variable InfluenceParticlePusher inside the class of FieldBackgroundE is false. If users wish to include the influence of background electric field in simulation, the users must change InfluenceParticlePusher's value to true. The same method applies to the other field quantities but the InfluenceParticlePusher variable is inside the class of FieldBackgroundB or FieldBackgroundJ. The structure of classes are the same for all field quantities.

4.3 Configuration file

The configuration file in PIconGPU is a file containing the information on simulation size, time and frame of simulation. Moreover, adjusting the configuration allows user to call built-in plugins relate to the outputs of simulation such as built-in density plot or energy distribution data. This file is named by `.cfg`.

4.3.1 General Configuration

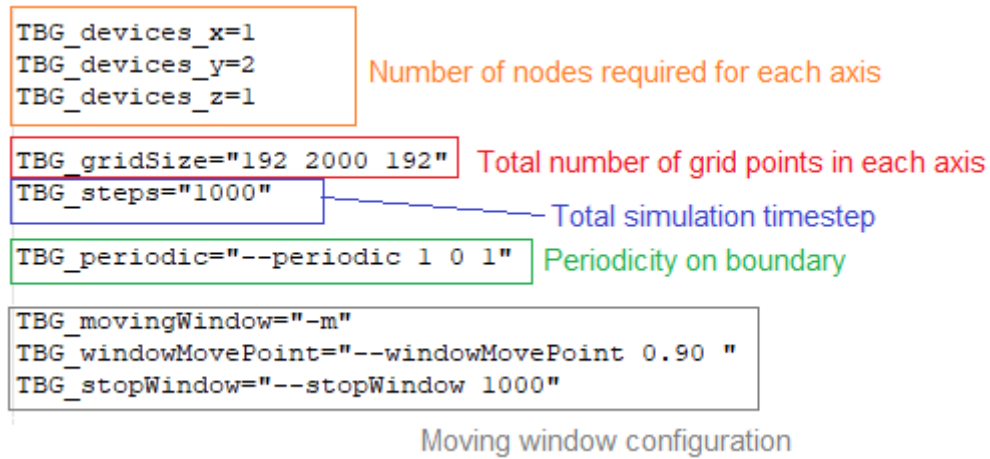


Fig 4.11 Simulation size and moving window configuration

In this case, as shown in Fig. 4.11, `TBG_devices_x` denotes the number of GPU nodes requires for x direction to the job scheduler for execution of our simulation. Therefore, we require 1 GPU in x and z direction and 2 GPUs for y direction. The resultant configuration can be illustrated as Fig. 4.12. if the simulation window is fixed. The number of GPUs available will allow larger simulation window.

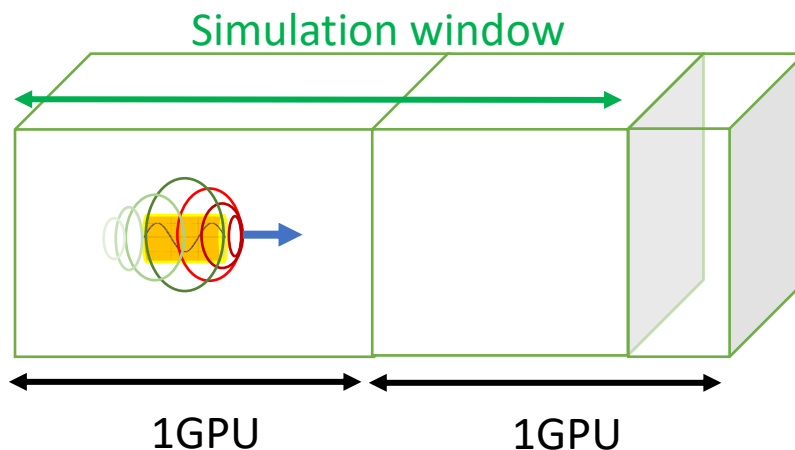


Fig 4.12 Simulation window for non-moving configuration with 3 GPUs

`TBG_gridSize` defines the total number of grid points on x, y and z direction respectively. In our example, we simulate the system with 192 grid points in x and z direction while there is 2000 grid points in y direction which is the direction of laser propagation.

The line `TBG_periodic` defines periodicity at the boundary of simulation window where 1 denotes periodicity and 0 denotes non-periodicity. In the sample, `--periodic 1 0 1` means that the simulation implements periodic boundary condition in x and z direction.

For the simulation that requires long simulation size that GPUs memory storage in our system is not suffice, we can implement moving window option by including the line `TBG_movingWindow= "-m"`. The simulation window will move in y direction with light speed after a short pause. The short pause before window of simulation begins to move comes from the line `TBG_windowMovePoint` which the numerical value used in this case is 0.9. This line means that window will move after a virtual particle from the leftmost of window, at the initial time, have propagated with lightspeed to 0.9 length of simulation window. The last line in Fig.() defines the total PIC cycle, or timestep that simulation window will stop moving. However, moving window configuration also requires at least 2 GPUs in y direction as the diagram of simulation window is not the same as fixed window case.

In this case, the window also propagates in y direction. The transparent boxes are some portion of another GPU running as the reserved space for simulation awaits to appear in simulation window as it propagates. In case of two GPUs in y direction, the configuration for moving window is illustrated as Fig. 4.13.

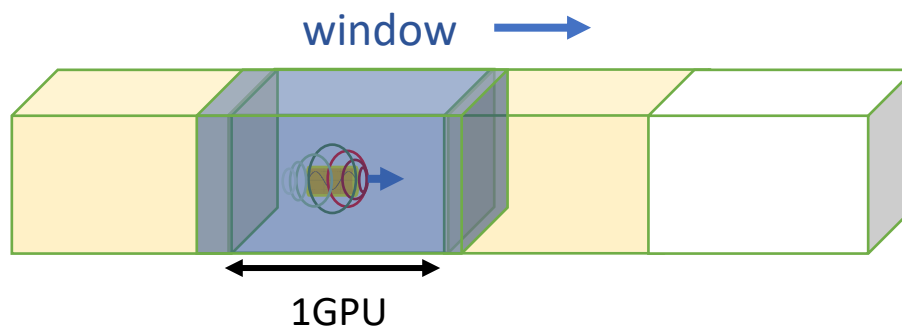


Fig 4.13 Simulation window for 2 GPUs node and moving window configuration

4.3.2 Plugins Configuration

As mentioned above, the configuration file allows user to call PIconGPU's plugins. The example for calling pngwriter plugin is shown in Fig. 4.14.

```
# png image output (rough electron density and laser preview)
TBG_pngYX="--e_png.period 50 \
          --e_png.axis yx --e_png.slicePoint 0.5 \
          --e_png.folder pngElectronsYX"
TBG_ionpngYX="--i_png.period 100 \
             --i_png.axis yx --i_png.slicePoint 0.5 \
             --i_png.folder pngElectronsYX"
```

Fig 4.14 PNG density plot plugin creation

The lines `TBG_pngYX` is command to construct a new plugin `TBG_pngYX`. The attributes of this plugin are `e_png.period 50`, `e_png.axis yx`, `e_png.slicepoint 0.5` and `e_png.folder pngElectronsYX`. The first attribute states that the pngwriter are called every 50 PIC cycles. Note that “e” in “`e_png.period`” clarifies that the program pngwriter are used for species with labelled “e”. This label can be adjusted freely in parameter file `speciesDefinition.param`. The second and third attributes, `e_png.axis yx` and `e_png.slicepoint 0.5`, mean that pngwriter plot particle density of species “e” in yx plane which lies at the middle of simulation in z direction. The `slicepoint` can be adjusted to translate the plane of interest on the remaining axis of simulation which is z axis in this case. The last attribute `e_png.folder` defines the output folder for this plugin.

Another example for plugin configuration is for energy histogram plugins. A section containing energy histogram plugin in configuration file is shown in Fig. 4.15.

```
# energy histogram (electrons, [keV])
TBG_e_histogram="--e_energyHistogram.period 50 \
                --e_energyHistogram.binCount 2048 \
                --e_energyHistogram.minEnergy 0 --e_energyHistogram.maxEnergy 20000 \
                --e_energyHistogram.filter all"
```

Fig 4.15 Definition of energy histogram’s plugin

This plugin has following properties:

- Name: `TBG_e_histogram`
- `e_energyHistogram.period 50`
Energy histogram is constructed for every 50 timestep after initiation.
- `e_energyHistogram.bincount 2048`
The energy histogram divides the energy into 2048 channel covering energy range from minimum energy to maximum energy.
- `e_energyHistogram.minEnergy 0`, `e_energyHistogram.maxEnergy 20000`
The kinetic energy of particles presented in the histogram ranges from 0 keV to 20000 keV.
- `e_energyHistogram.filter all`
All particles of species “e” are count in construction of histogram.

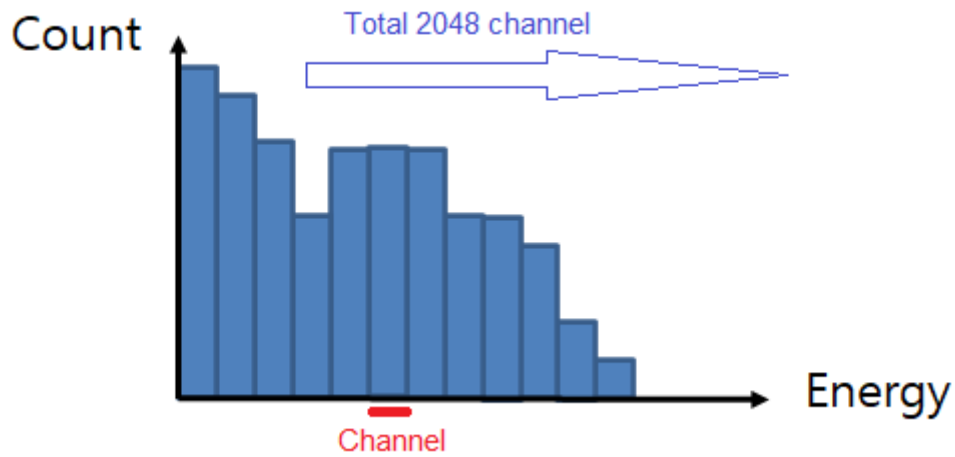


Fig 4.16 Energy distribution channel illustration

In computer programming, we can construct functions at the beginning of the file, however, actual implementation of the functions is not mandatory. After the plugins are defined at the beginning of configuration file, implementation of plugins is summarized at the bottom of file. The lines that summarized plugins are shown in Fig. 4.17.

```
TBG_plugins="!TBG_pngYX          \
            !TBG_ionpngYX       \
            !TBG_e_histogram    \
            !TBG_e_PSyPy        \
            !TBG_e_macroCount   \
            !TBG_hdf5           \
            !TBG_e_Calorimeter"
```

Fig 4.17 Summarizing lines of plugins

4.3.3 Program Parameters

The last section of configuration file is the section that summarizes all simulation parameters and plugins before sending the program to the job scheduler. The example of this section is shown in Fig. 4.18.

```

#####
## Section: Program Parameters ##
#####

TBG_deviceDist="!TBG_devices_x !TBG_devices_y !TBG_devices_z"

TBG_programParams="-d !TBG_deviceDist \
                  -g !TBG_gridSize   \
                  -s !TBG_steps      \
                  !TBG_movingWindow \
                  !TBG_periodic     \
                  !TBG_plugins      \
                  --versionOnce"

# TOTAL number of devices
TBG_tasks="$(( TBG_devices_x * TBG_devices_y * TBG_devices_z ))"

"$TBG_cfgPath"/submitAction.sh

```

Fig 4.18 Program parameter part in configuration file

4.4 Simulation Setup

First step for setting up a simulation is to determine the appropriate simulation size. The simulation size is determined from the number of grid points and grid separation in each direction. If simulation size is small, the boundary will influence the results. If the simulation size were too large, the simulation will contain large number of plasma particles, resulting in insufficient computational resources. Moreover, the perturbation of plasma particle inside LWFA occurs at the middle of simulation window. Plasma particles situated far apart from the middle of simulation are likely to be less perturbed. So, larger simulation size can lead to total waste of computational resources.

To find appropriate simulation size, first consider laser's wavelength. The wavelength of laser is set to 800 nm which is the longest wavelength for invisible – light laser. The reason to fix the wavelength at the highest value is the grid separation. To simulate the effect of laser's oscillating electric field in the simulation, we require 20 grid points for y direction in one wavelength of laser. Therefore, the result is that the grid separation in y direction is 40 nm. The grid separation in x and z direction is kept at default value of 200 nm. Second, the total number of grid points is determined by observation on density plot. At the highest laser strength parameter, $A=10.0$, the maximum blowout radius of electrons is observed, and we choose that the blowout should not exceed the boundary. So, the electron blowout of laser strength parameter $A=10.0$ at the lowest plasma density in the investigation 10^{23} m^{-3} is observed. It requires that the grid point must be at least 256 points in x and z direction where number 256 comes from the power of 2. Next, the number grid points in z direction is 2048 which is the maximum number of grid points. By considering the case of highest number of plasma particle which consumes computational resource the most, we found that the number of grids point in power of 2 should not exceed 2048. Since the

computational resources are limited and the self-injection phenomenon occurs at approximately 300 fs after LWFA initiation, the moving window configuration is implemented. Moving window configuration requires at least 2 computation nodes in direction of propagation. Since NARIT's CHALAWAN provides maximum parallel computation of 2 GPUs. The configuration of simulation window and size is finalized. The simulation window is illustrated in Fig. 4.19. Finally, the timestep separation used for this simulation is 0.1 fs.

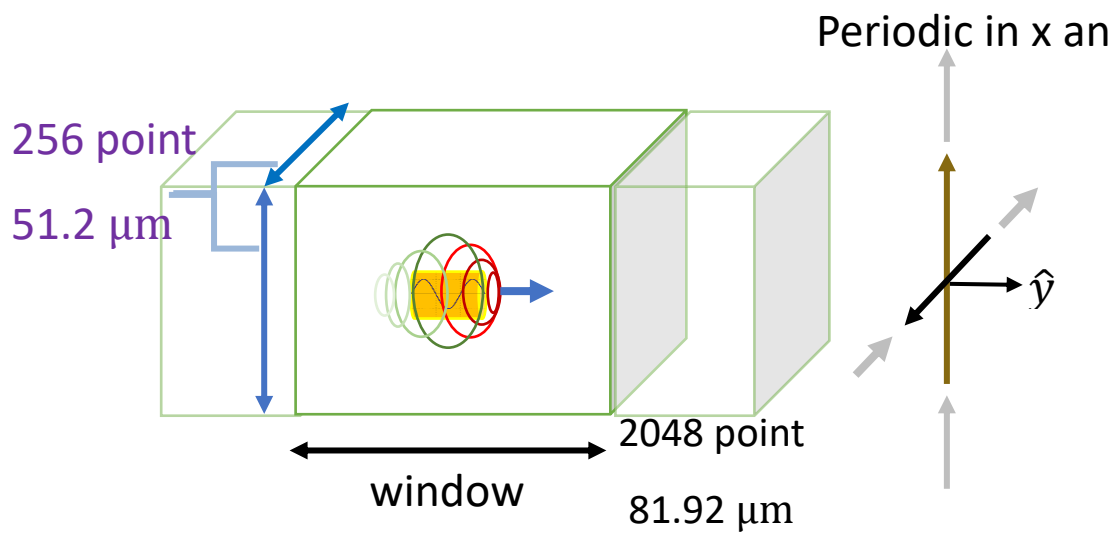


Fig 4.19 Simulation size set up

Second step is definition of the laser profile. Since the laser's wavelength of 800 nm gives the largest grid separation in y direction, then the wavelength of 800 nm is used throughout the project. Laser's profile used in this project is the most basic profile, gaussian distribution. The laser profile is illustrated as Fig. 4.20

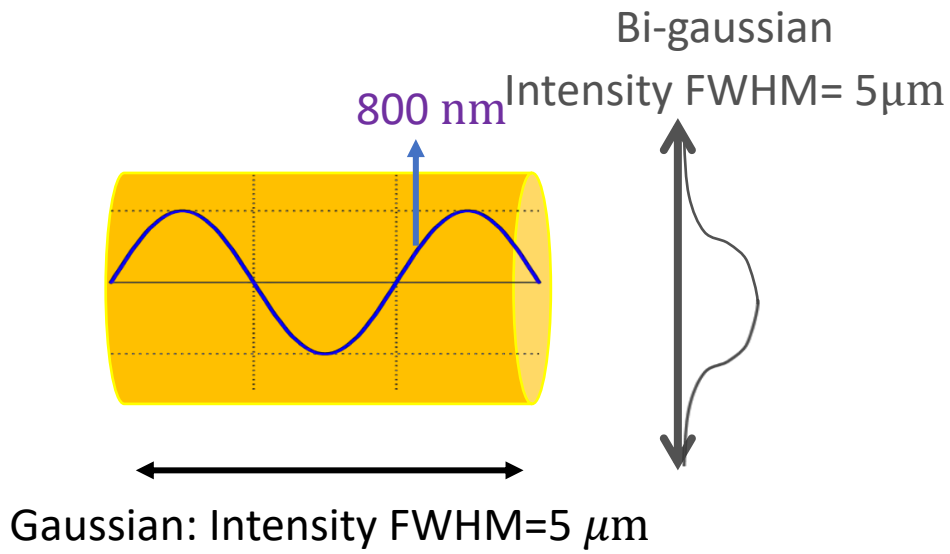


Fig 4.20 Laser profile

The profile is gaussian in y direction with full width half maximum of $5\mu\text{m}$. In the radius direction, the profile is Bi-gaussian distribution in x and z direction. From the characteristics of ponderomotive force, the laser will blow charged particle away from the laser axis. The diagram for laser interaction with plasma is illustrated in Fig. 2.6

CHAPTER FIVE: RESULTS AND DISCUSSION

In this chapter, the simulation results from PIConGPU on Linux operation system are presented. The systems are simulated in NARIT's Supercomputer, Chalawan using 2 GPU nodes accounting for 8 graphic processing units. The simulation's grid size is 256×2048×256; the number of grid points are larger in y direction. The cell' sizes are 0.4 μm in x and z directions and 2 μm in y direction. The timestep size is 0.1 fs. Parameters for simulation are input using .param files. In our simulation, only 3 parameters which are laser's strength parameter or normalized vector potential magnitude $A_0 = \frac{ea_0}{m_e c^2}$ (CGS) where a_0 is the magnitude of vector potential, plasma density and background magnetic field are adjusted. Other parameters are fixed at the most appropriate value such as simulation volume, shape of laser pulse, interpolation of field and force inside the simulation.

5.1 Electrons and ions motion inside laser-plasma wakefield accelerator

Inside laser-plasma wakefield accelerator, charge particles are excited into motion by laser's electromagnetic field. The force acting on each charge particle is Lorentz force which is the combination of electric and magnetic force by the formula (SI unit)

$$\mathbf{F} = q\mathbf{E} + q\mathbf{v} \times \mathbf{B}.$$

In vacuum, electromagnetic wave including laser's magnetic field part \mathbf{B} have smaller amplitude compare to the electric field \mathbf{E} by the factor c describing speed of light in vacuum. Therefore, laser's magnetic field contribution can be neglected except for relativistic particles whose speed is near light speed. Therefore, leading order of low-energy electrons comes from electric field. Since electric field generated by laser pulse oscillates, leading order motion is oscillation. However, electrons are observed drifting away from laser pulse in simulation. The repulsion force from second order motion, ponderomotive force is observable as well in our simulations. Ponderomotive force results in repulsion of electrons and ions inside wakefield accelerator. Theoretically, ponderomotive force is proportional to charge per mass $\frac{q}{m}$. Hence, the plasma ion's motion is far slower than electron. In case of hydrogen plasma, motion of ions is approximately 3 million times slower than electrons. Therefore, ions are considered motionless inside laser-wakefield accelerators. The motion of electrons and ions can be observed by density plot as shown in Fig 5.1.

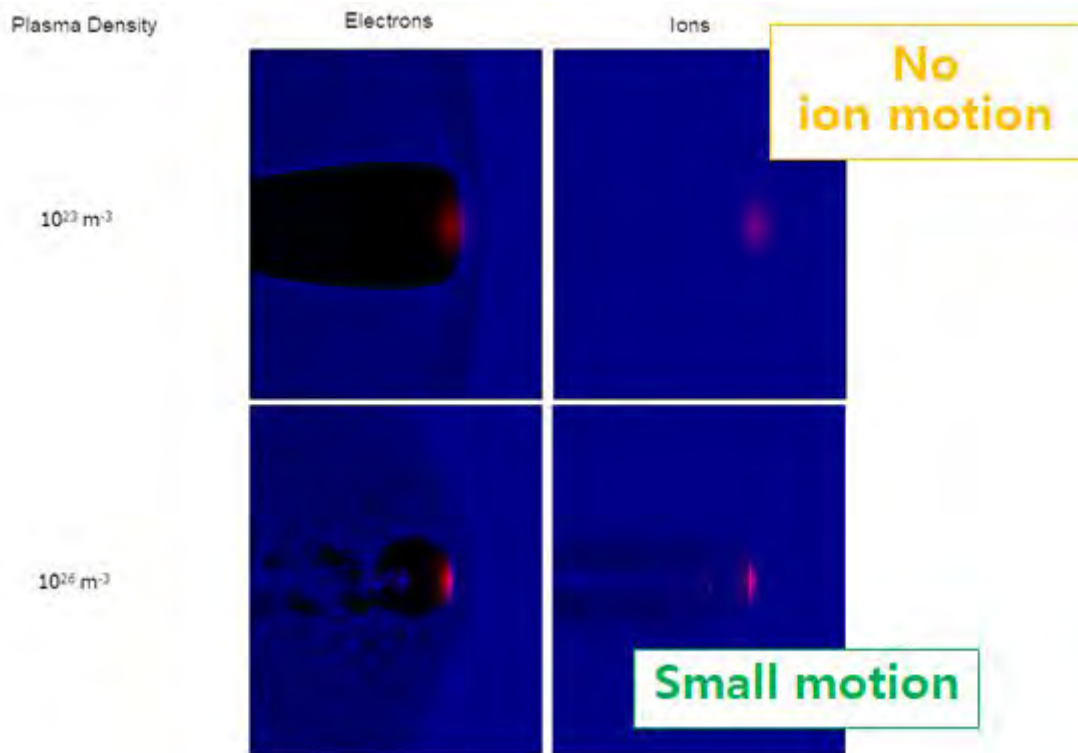


Fig 5.1 The density plots for electrons and ions inside laser-plasma wakefield accelerator obtained in simulation with laser strength parameter $A=10$ at times 300 fs after initiation.

The density plots are shown for minimum and maximum value of plasma density used in this study, which are 10^{23} and 10^{26} m^{-3} respectively. Simulations are done in 3-dimensional space while the density pictures are obtained by longitudinal cross section at the middle of accelerators. For each plasma density, the plots for electrons are on the left and ions density plots are on the right. Blue regions indicate occupancy of particles and red shade depicts the magnitude of laser's electric field. The density plot clearly shows that ions inside wakefield accelerator are less perturbed compared with the electrons inside the same accelerator. The laser parameter of $A=10$ is the maximum value being investigated in this study.

From the results, we find that electrons are blown away from the laser and the generation of plasma wake is observed. Simulation setups permit the generation of plasma wake and other important phenomena which are laser depletion and self-injection. The generation of plasma wake occurs at initial state of accelerator. Laser pulse are directed into plasma volume before electrons are repelled out by laser's field while ions are approximately motionless generating positive space charge behind the laser leading pulse. The space charge called "bubble" attracts nearby electrons. Electron density waves are developed by oscillation of electrons by positive space charge attraction and result in plasma wake and its field, wakefield. After the development of wakefield, some electrons are attracted to positive space charge and gain momentum in laser's direction.

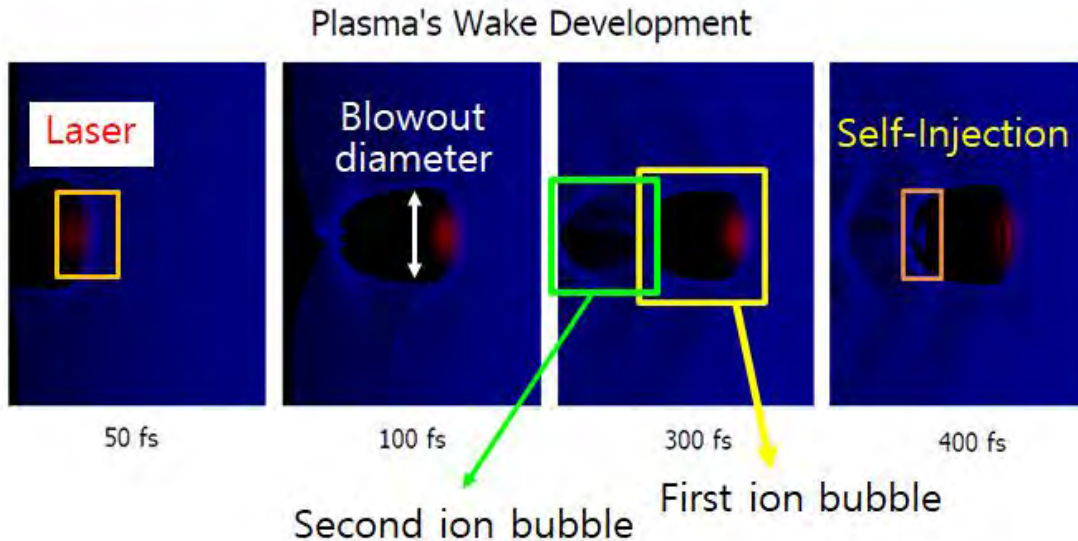


Fig 5.2 The development of plasma wake inside laser-plasma wakefield accelerator from the simulation by PICongGPU with laser strength parameter $A=10.0$ and plasma density of 10^{25} m^{-3} .

In Fig 5.2, blue tone represents density of electrons at the site. The density is plotted for time 50, 100, 300 and 400 fs after initiation. At the beginning of the development process, electrons are repelled out by laser resulting in large space charge tube as the picture at 50 fs. At 100fs, as laser propagates, the positive space charge attracts the electrons toward the axis of the tube, resulting in the closure of the space charge behind laser pulse. The shape of space charge behind the laser pulse becomes “bubble” shape. Electrons pass one another by inertia after being attracted by the space charge and results in another bubble. Bubbles are generated along the line of laser propagation as the plot at 300 fs. The plasma wake from the chain of bubbles generates wakefield for acceleration. At 400 fs, small portion of electrons have high energy and propagate with near-light speed. Self-injection of electrons into the bubbles is observed at 400 fs.

The acceleration of electrons can be observed by energy distribution or phase space. In some cases, density plot show evidence of acceleration. Some electrons gain kinetic energy enough to catch the speed of laser pulse. Those electrons will move into the plasma wake which is observed in simulation result in Fig 5.2 at 400 fs. Therefore, density plot from the simulation indicates that PICongGPU is capable enough to reproduce laser-plasma wakefield accelerator and its phenomenon, at least, electrons acceleration.

The electrons acceleration can be observed by energy distribution over the time inside laser-plasma wakefield accelerator.

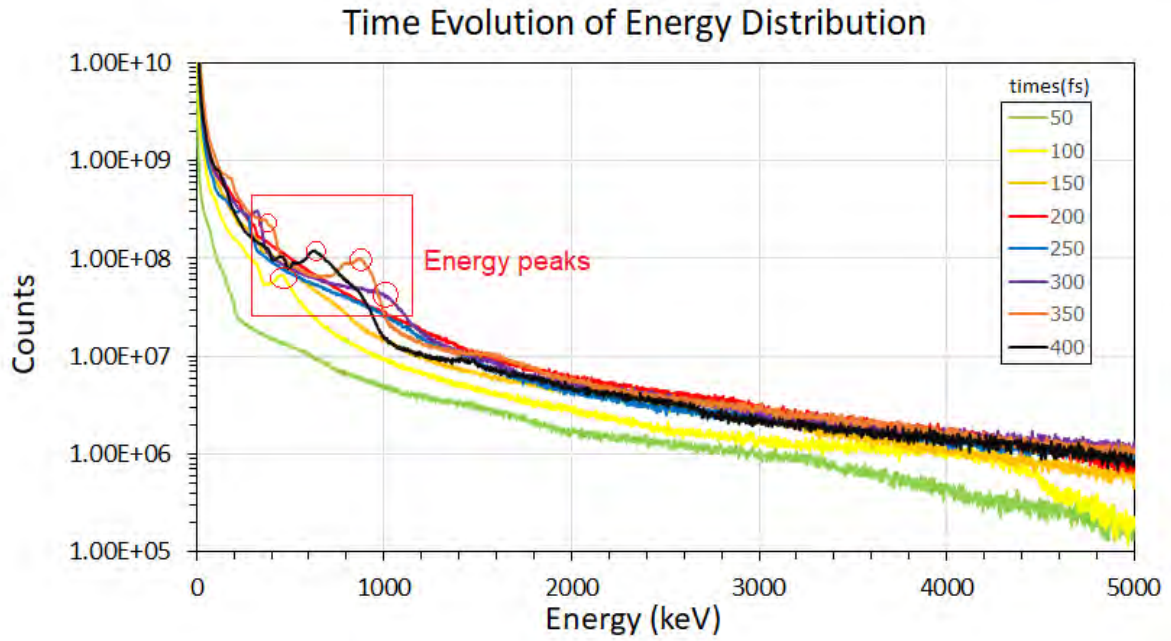


Fig 5.3 The evolution of energy distribution over time for laser parameter $A=10.0$ and plasma density 10^{25} m^{-3} .

Each line in Fig. 5.3 represents the energy distribution at time 50 to 300 fs with 50 fs separation. The distribution shows electron's energy peaks which are identified by circles. These energy peaks are evidence for trapping phenomena.

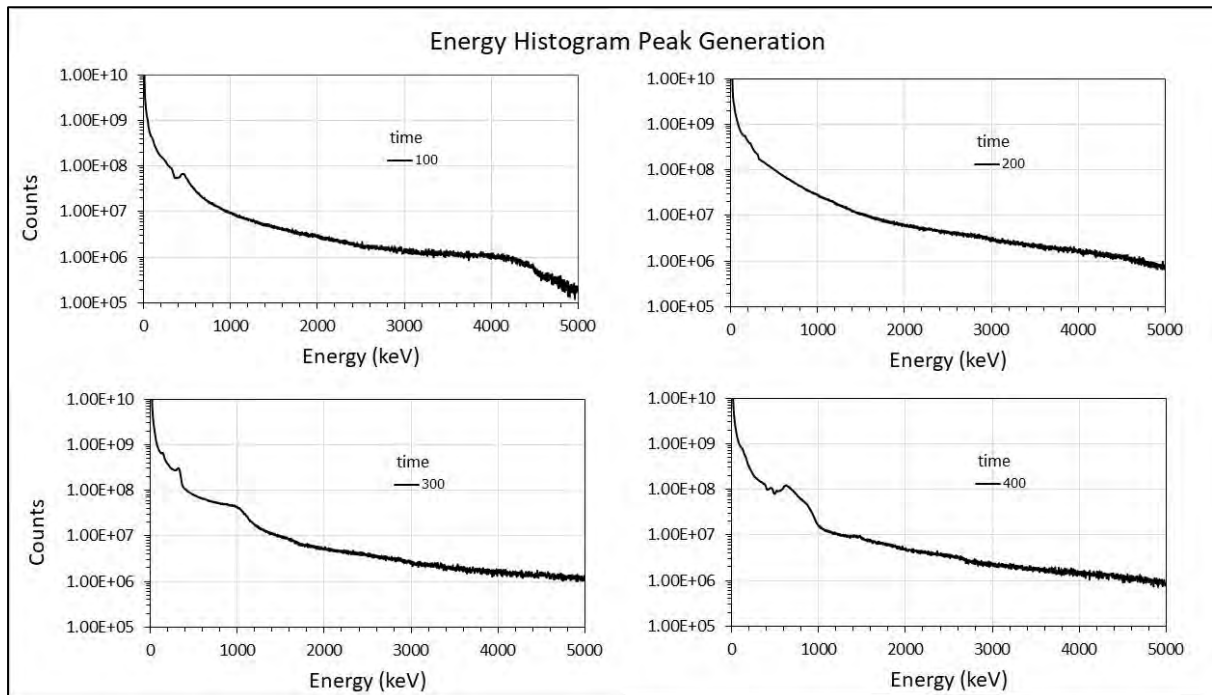


Fig 5.4 Separate plot of energy distribution from 100 fs to 400 fs after initiation of wakefield accelerator with laser strength $A=10.0$ and plasma density 10^{25} m^{-3} .

From Fig 5.4, the evolution from 200 fs to 400 fs clearly shows the generation distribution peak. The occurring peak suggests some mechanisms that gather some portion of electrons and have effect on their speed.

5.2 Plasma Density Effects on Blowout Radius and Shape

First, the author investigates the effects of plasma density on blowout radius and shape of wake which can be shown in plasma density plot.

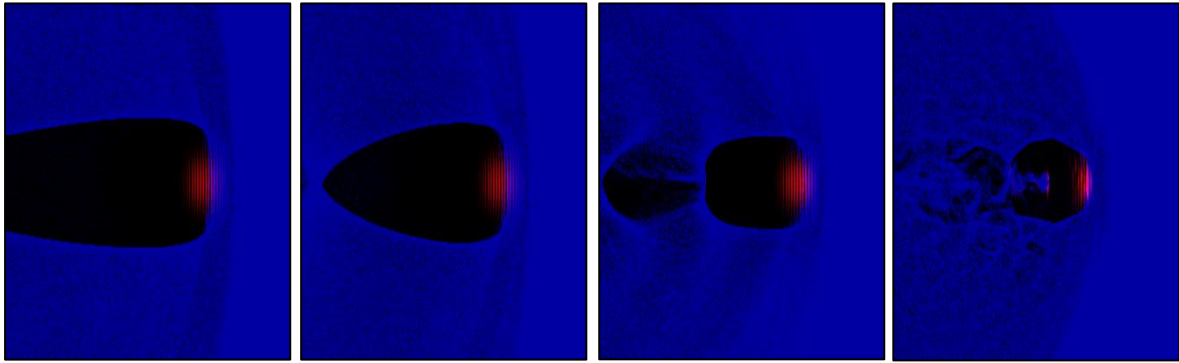


Fig 5.5 Electron density plot for LWFA at plasma density 10^{23} , 10^{24} , 10^{25} and 10^{26} m^{-3}

In Fig. 5.5, from left to right, are the density plot for wakefield accelerator's simulation at plasma density of 10^{23} , 10^{24} , 10^{25} and 10^{26} particles/ m^3 respectively using laser strength parameter $A=10.0$, and without axial magnetic field. The electron density is plotted in blue color. The plots clearly show that plasma density affects the blowout.

Fig 5.5 shows that the space charge becomes narrower and shorter for denser plasma. The results agree with simple reasoning. Ponderomotive force which depends on the gradient of squared amplitude electric field is bounded by a maximum value at radii distance $r = \frac{\sigma_r}{\sqrt{2}} = 0.707\sigma_r$ with maximum value of ponderomotive force being $\mathbf{F}_p = \frac{A_0^2}{c^2} \frac{e^2}{4m\omega^2} \frac{\exp\left(-\frac{1}{2}\right)}{\sqrt{2}\sigma_r} \hat{\mathbf{r}}$. Then the kinetic energy of dispersed electrons is limited to some value. However, attraction force from space charge increases as the density of plasma increases. Therefore, the electrons dispersion radius is reduced. Notice that in our simulation, laser's electric field is not confined to some radius but extend to infinity as the function $\exp\left(-\frac{r^2}{2\sigma_r}\right)$ yields non-zero value for all value of r . In that case, as mentioned by Wei Lu (2016) (4), only the portion of electrons inside the laser's radius are affected. After they are repelled out further than laser's radius, the electrons will not be affected by laser anymore, and will gradually lose momentum in the radial direction due to attraction of space charge. Our simulation results have shown that wakefield accelerators with infinitely large laser cross section are also permitted.

For further investigation of blowout radius, the author simulates wakefield accelerator in different plasma density values and measures the maximum blowout radius of plasma density wake for plasma density range 10^{23} to 10^{26} m^{-3} .

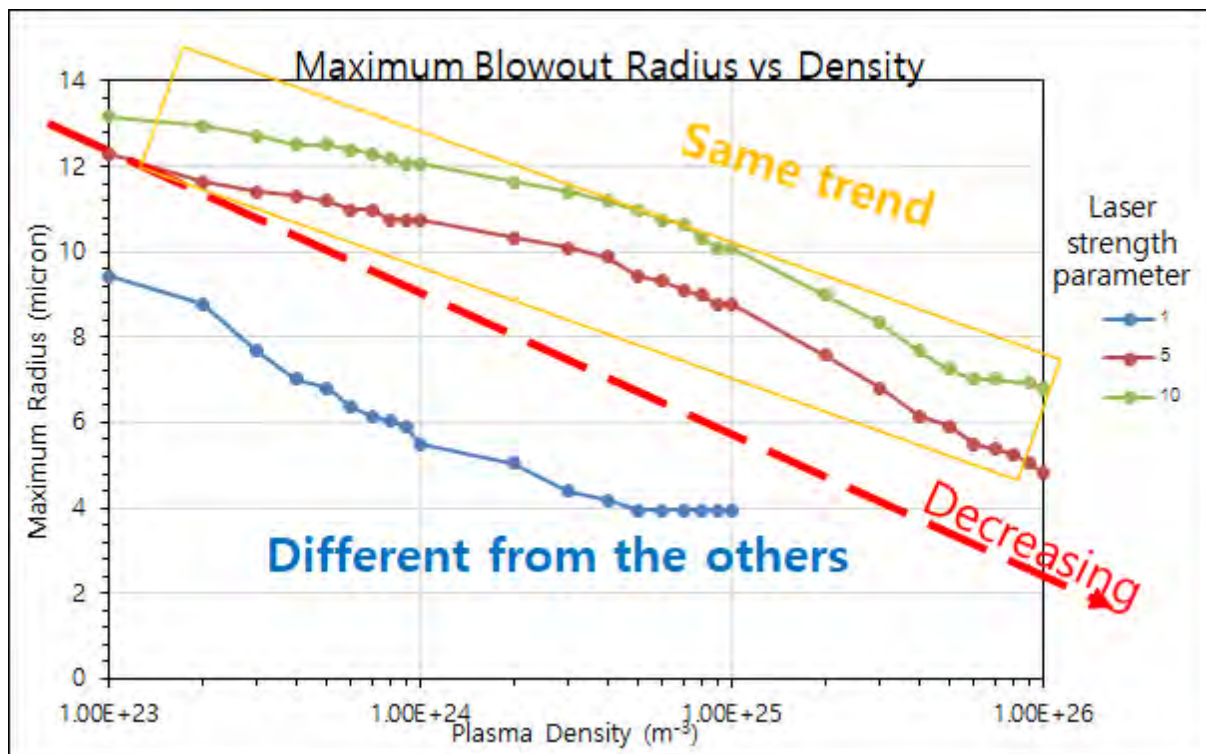


Fig 5.6 Maximum electron blowout radius inside LWFA for plasma density range 10^{23} m^{-3} to 10^{26} m^{-3}

Fig. 5.6 shows the value of maximum blowout radius measured from simulation using PIconGPU on NARIT's CHALAWAN for plasma density range 10^{23} to 10^{26} m^{-3} . Each line represents distinct value of laser strength parameter $A= 1.0, 5.0$ and 10 . Plasma density is displayed in logarithmic scale. The measurements are conducted at timestep 1500, or 150 fs after initiation. The experiment results for plasma density above 10^{25} m^{-3} with $A=1.0$ is excluded because their blowout radius is unable to identified by incomplete electron blowouts.

From the relation of maximum blowout radius and plasma density. Variations of radius for laser parameter 5.0 and 10.0 resemble each other, while laser parameter 1.0 obviously differs from the others. Similarity in laser parameter 5.0 and 10.0 is the result from saturation of blowout phenomenon. For small laser parameter, laser cause small perturbation in plasma volume; only small portion of electrons are blown out from laser pulse. Higher power laser means larger blowout portion in electrons. Since electron number is limited by plasma density value, very strong laser will completely blow out the electrons in its path. The evidence for different blowout mode can be shown by density plot.

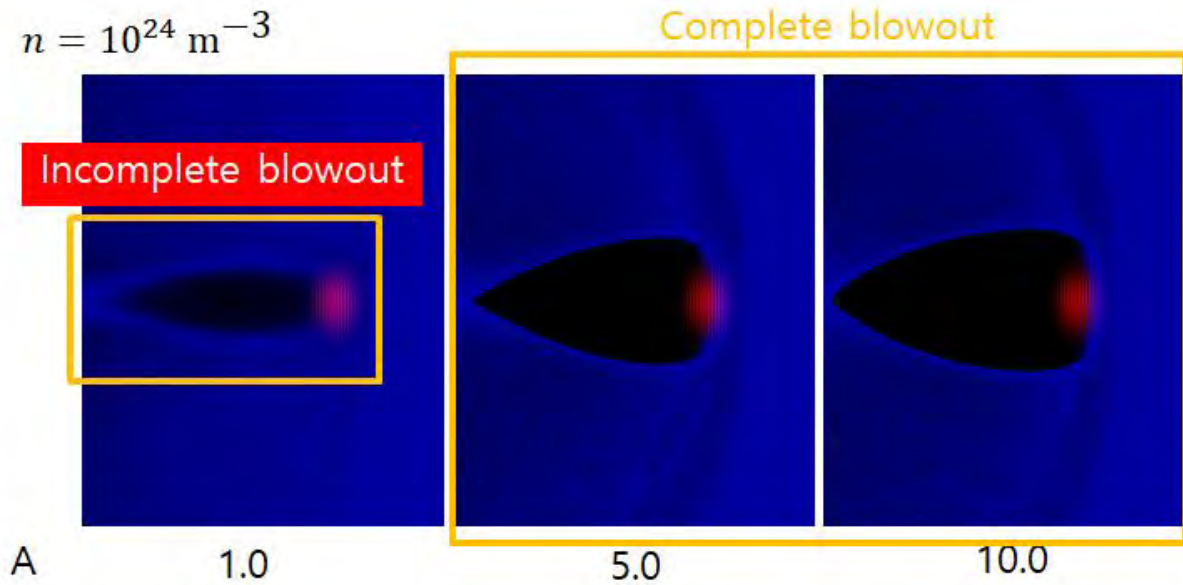


Fig 5.7 Observation on mode of blowout in LWFA

From left to right, electron density plot at 150 fs after initiation for laser parameter $A=1.0$, 5.0 and 10.0 , respectively, at plasma density value 10^{24} m^{-3} . Blue shade represents density of electrons and red color represents the electric field magnitude of laser. Electron density plots shows vast different between weak laser pulse and strong laser pulse. Some electrons are located around the axis of laser propagation for weak laser pulse which is large number of small blue dot behind the pulse. Meanwhile, strong laser pulse $A=5.0$ and 10.0 completely repel the electrons behind the pulse resulting in dark space with sharp contour at the edge of bubbles.

The different modes of blowout can be observed in the above picture, where complete blowout occurs at laser parameter 5.0 and 10.0 . Whereas, for laser parameter $A=1.0$, the electrons are not completely blown out from laser pulse, resulting in blur region at the edge of blowout in density plot. This observation indicates that laser strength also has an important role in controlling wakefield accelerator of laser-type.

5.3 Plasma Density Effects on Electrons Acceleration

First, investigations on kinetic energy distribution for laser parameter of value 1.0 , 5.0 and 10.0 are conducted. Plasma densities range from 10^{23} to 10^{26} m^{-3} are used for the simulations. The energy histograms for laser strength parameter $A=10.0$ are shown for some plasma density values in Fig. 5.8. The energy distribution is typically similar to the distribution of density 10^{23} m^{-3} . The distribution resembles diffusion process.

Energy Distribution

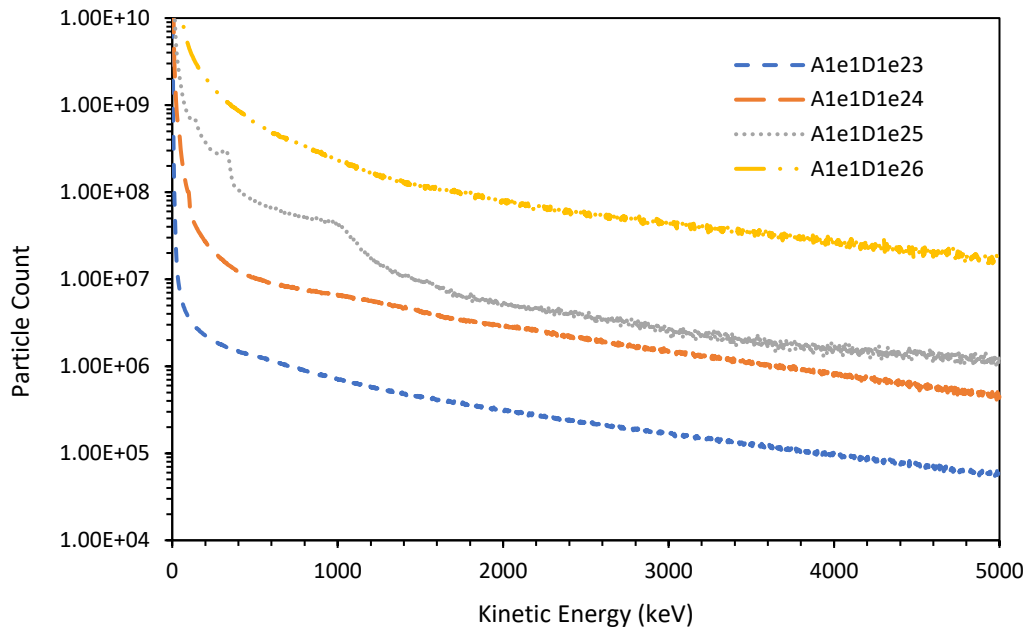


Fig. 5.8 Kinetic energy distribution of electrons inside LWFA with laser parameter $A=10.0$ for specific plasma density value of 10^{23} m^{-3} to 10^{26} m^{-3} .

Each line in Fig. 5.8 represents distribution for one plasma density value labeled by format “A + value of A + D + Value of plasma density [unit m^{-3}]”. Energy histogram indicates abnormality for plasma density value of 10^{25} m^{-3} where variations of electron number over the kinetic energy differ from the others.

Since the energy distribution of electrons shown above resembles for plasma density value 10^{23} , 10^{24} and 10^{26} , the distribution for density 10^{25} can be predicted. From simulation data, the number of particles at specific kinetic energy of 10^{24} plasma density is approximately 10 times the number for 10^{23} density. The prediction for plasma density of 10^{25} and its simulation values are compared.

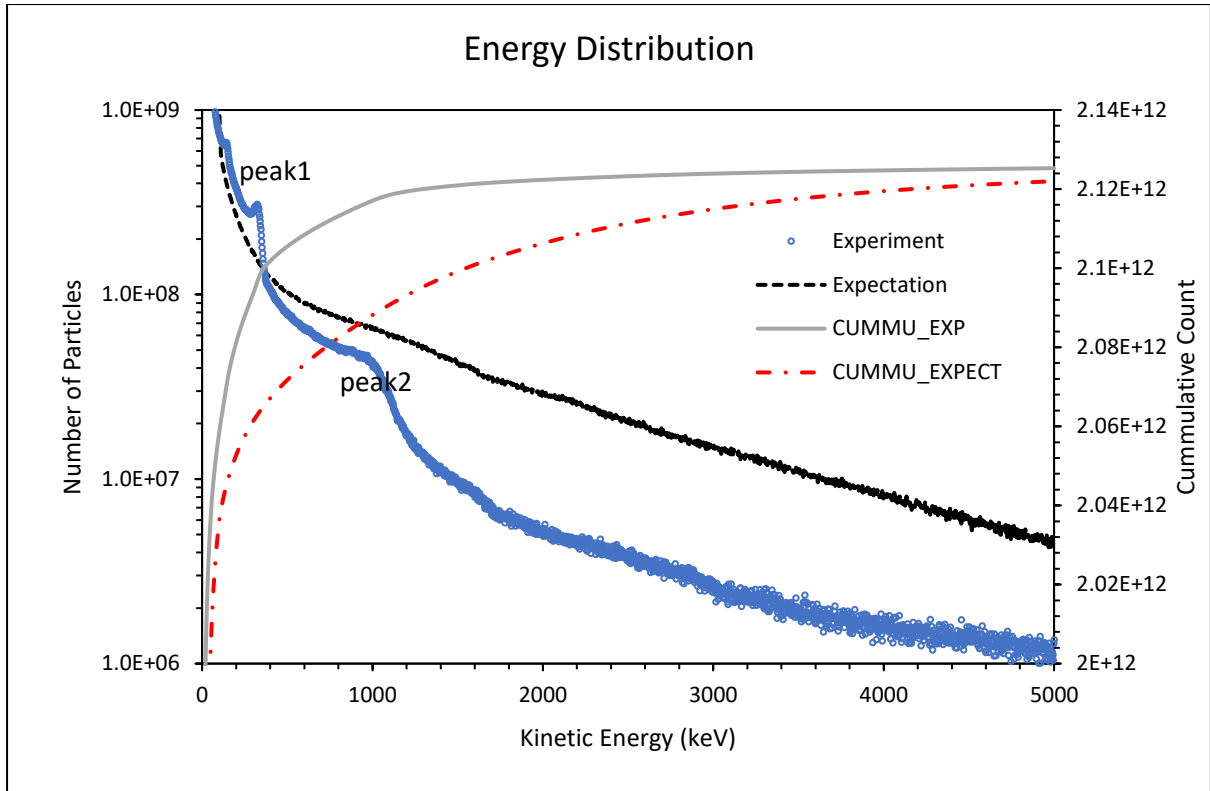


Fig 5.9 Energy distribution from simulation and predicted value from normal trends of plasma wakefield accelerator with $A=10.0$ and plasma density 10^{25} m^{-3} at 300 fs after initiation.

Fig 5.9. shows that the prediction is an underestimation for low kinetic energy up to, approximately, 300 keV. After that, the prediction gives an overestimation. Consequently, the cumulative count for electrons are different. For simulation, most electrons have lower kinetic energy than predicted by the trends. Each peak identifies electron trapping phenomenon for periodic boundary condition.

Another simulation is conducted for the same configuration but with non-periodic boundary condition to see differences in energy distribution. In wakefield accelerator, boundary condition may affect the acceleration process of electrons. This is an experiment to check and see if there is a boundary effect in the simulation.

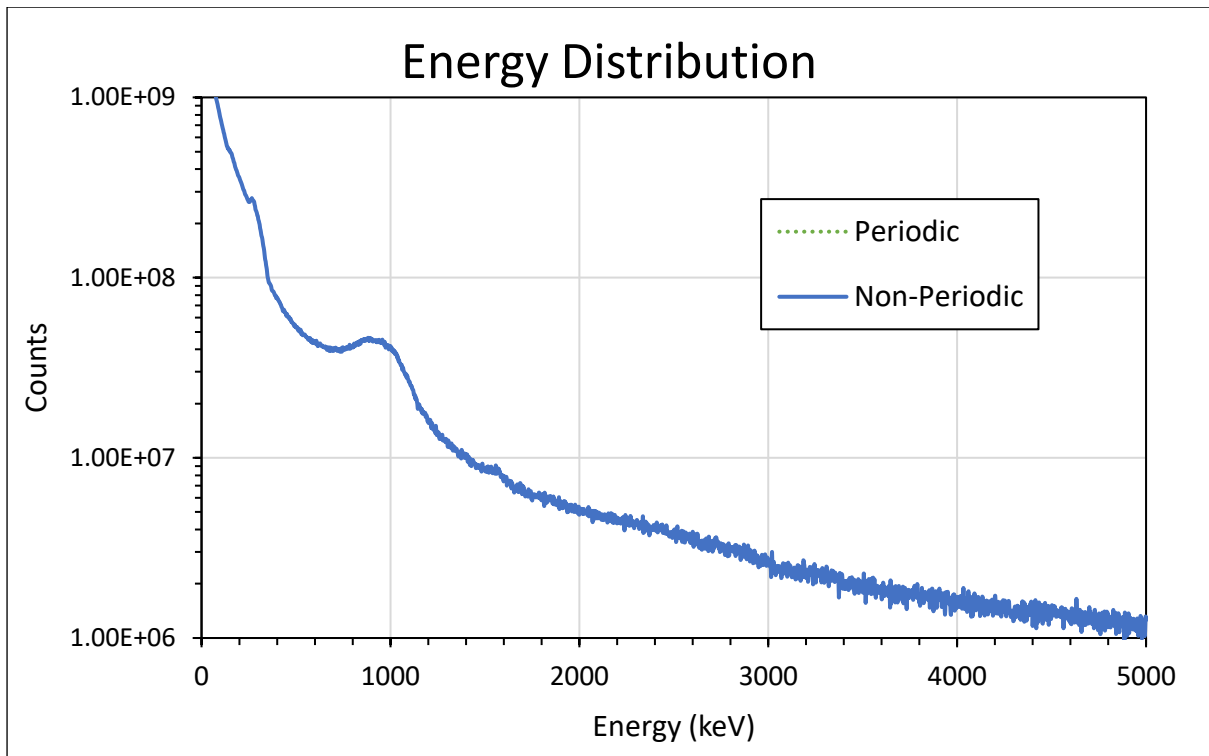


Fig 5.10 Comparison of energy distribution for plasma density 10^{25} m^{-3} with different boundary condition in x and z axis.

The graph in Fig. 5.10 indicates insignificant difference in periodic and non-periodic boundary condition. It is an evidence that peak generation in energy distribution is not affected by periodic condition of wakefield accelerator in a quantitative manner. Since there are no significant qualitative differences in energy distribution for periodic and non-periodic boundary condition, all following simulations are conducted with periodic boundary condition to preserve computational resources.

After that, investigations are conducted using the same periodic boundary condition but with laser strength $A=1.0$. The results are shown in Fig. 5.11.

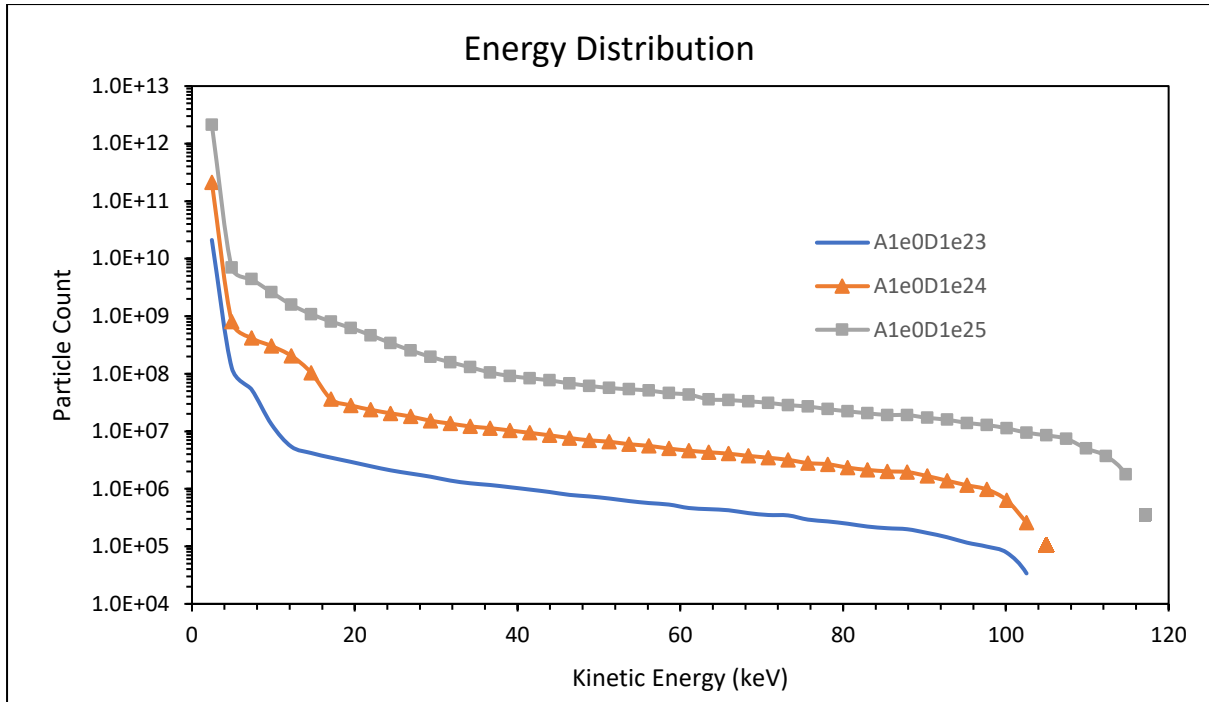


Fig 5.11 Kinetic energy distribution of electrons inside LWFA with laser parameter $A=1.0$ for plasma density range from 10^{23} m^{-3} to 10^{25} m^{-3} at 300 fs.

Fig 5.11 shows that, qualitatively, overall distribution resembles Fig 5.8 except for plasma density of 10^{25} m^{-3} . However, in quantity, electrons all have energy below 120 keV which is far lower compared to those in Fig 4.8 that some electrons have reached 5000 keV in the same amount of time.

Investigation in energy distribution shows similarity to the case of $A=10.0$. The number also decreases in the same manner as in the previous case. It decreases dramatically at low energy then decreases in linear manner in logarithmic scale, suggesting power law decay. However, there is no particles found which results in rapid decline at approximately 100 keV. Notice that the acceleration in this case is much lower compared to prior case. Seemingly, the electrons acceleration is proportion to laser's strength.

Since wakefield can either accelerate or decelerate electrons in accelerator, observation on evolution of energy distribution should provide evidence for deceleration. The clues are found for simulation results from laser wakefield accelerator with $A=10.0$ and plasma density of 10^{25} m^{-3} . The results are shown in Fig. 5.12.

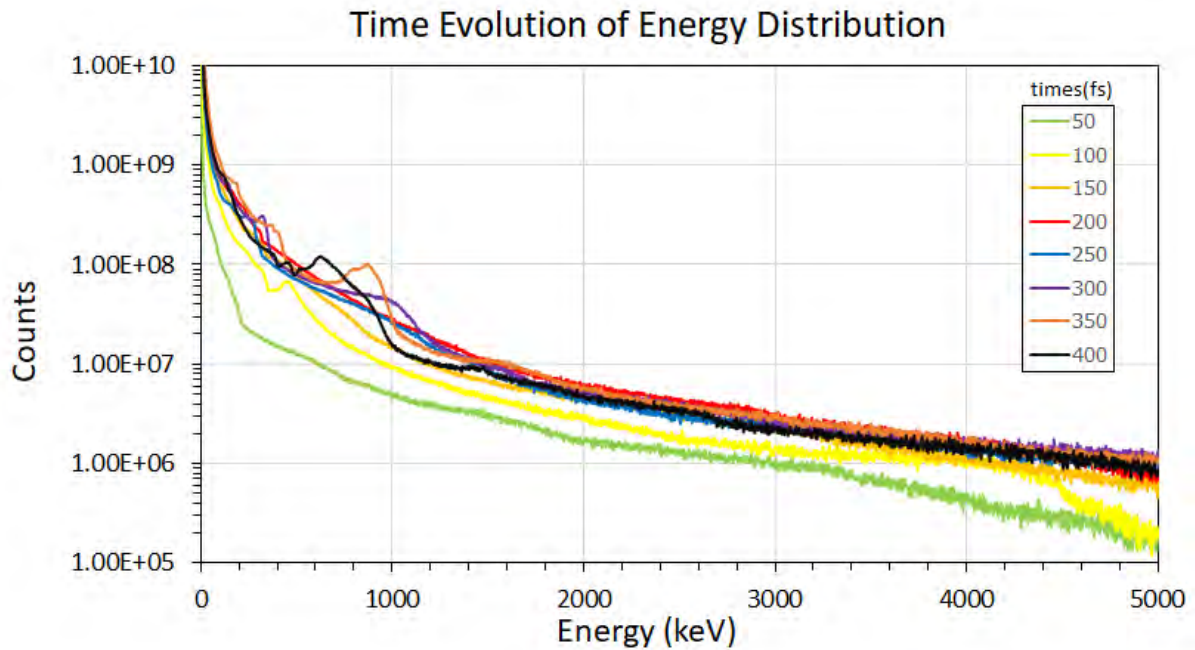


Fig. 5.12 Time evolution of electron's energy distribution for laser-type plasma wakefield accelerator with $A=10.0$ and plasma density 10^{25} m^{-3} from 50 to 400 fs, with 50 fs separation, after initiation.

Each line represents energy distribution at one time and the darker colors represent later time. The evidence of deceleration is presented for data from 250 fs to 400 fs. At 250 fs, electrons are being trapped and that results in peak at 1000 keV in 300 fs. However, at 350 fs, energy peak situates at approximately 800 keV and shifts to lower energy region until it becomes 600 keV peak at 400 fs. Evidently, some portions of electrons are decelerated in this time interval.

Fig 5.12 shows evidence that electrons are decelerated. Energy peaks at 1000 keV for 300 fs, 800 keV for 350 fs and 600 keV for 400 fs after initiation. Actually, only the translation of energy peak is not sufficient to deduce the deceleration, but in this case, energy distributions for energy higher than 1400 keV are approximately the same. The number of particles at 1000 keV also decreases as time increases from 250 fs to 400 fs while, at the same time, peak translates from 1000 keV to 600 keV. Note that this investigation also shows that the length of LWFA affects electron acceleration. Too long an accelerator can cause the electrons to decelerate and results in energy lowering of electron beam at the end of accelerator. Next concern is that plasma density may affect the acceleration and deceleration of electron. Some values of plasma density may be more appropriate for specific accelerator length and laser's strength. Plasma density is also a factor to determine dephasing length and pump depletion length. Dephasing length comes from the length that accelerated electrons will move out of acceleration phase in wakefield and stop being accelerated. Those electrons then experience deceleration by wakefield and lower their energy. Pump depletion length is the length scale for which laser's inside LWFA decrease its amplitude to $1/e$. The blowout of electrons become weaker for longer distance of laser propagation. Since both mentioned

lengths are inversely proportional to plasma density, therefore, too high plasma density or too long accelerator will cause a downgrade on LWFA. For a fixed length of the accelerator, like in this study, too high plasma density will result in dephasing and lowering of energy beam. To emphasize the importance of dephasing in wakefield accelerator, the energy distributions are investigated further.

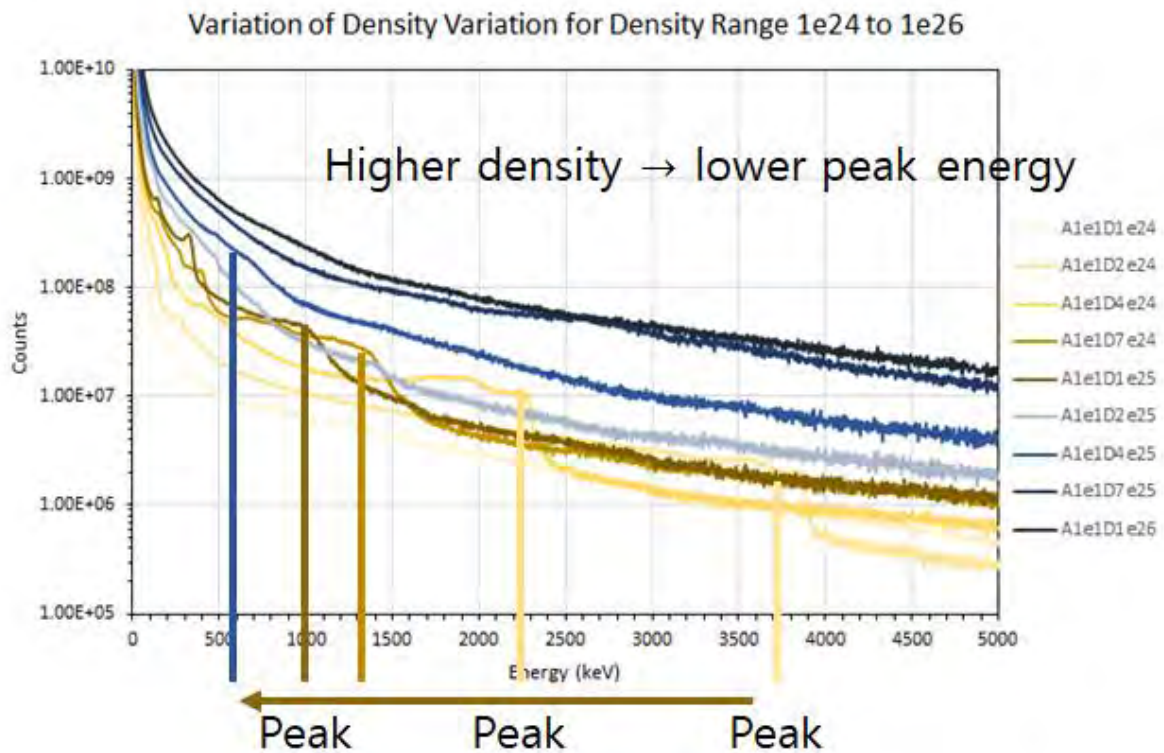


Fig 5.13 Variation of energy distribution at time 300 fs for LWFA of plasma density from 10^{24} to 10^{26} m^{-3} for laser strength $A=10.0$.

Consider Fig 5.13, the peaks identified in the distribution for plasma density of order 10^{24} - 10^{25} m^{-3} shows a tendency to have lower energy for higher plasma density. There is no conclusive evidence that peak translation comes from the fact that peaks are generated at lower energy or lowering of peak energy by deceleration processes. To identify the cause of this tendency, lowering of peak energy must be investigated for each plasma density.

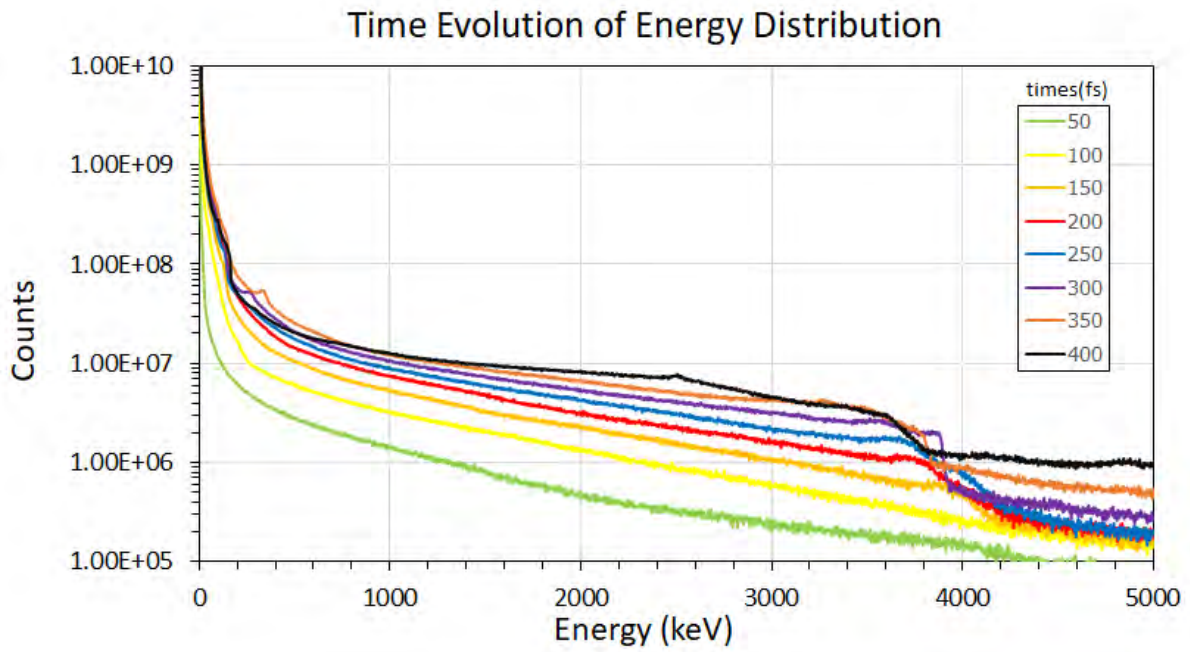


Fig 4.14A Time evolution of energy distribution from 50 to 400 fs for LWFA with plasma density $2 \times 10^{24} \text{ m}^{-3}$ and laser strength $A=10.0$.

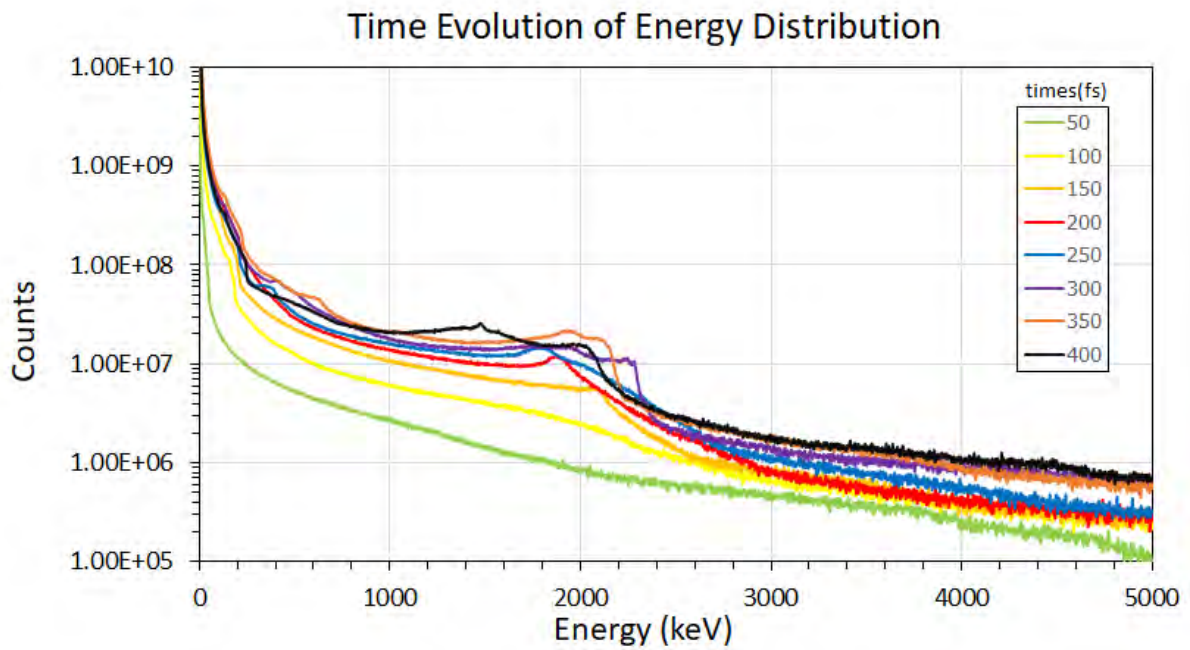


Fig 5.14B Time evolution of energy distribution from 50 to 400 fs for LWFA with plasma density $4 \times 10^{24} \text{ m}^{-3}$ and laser strength $A=10.0$.

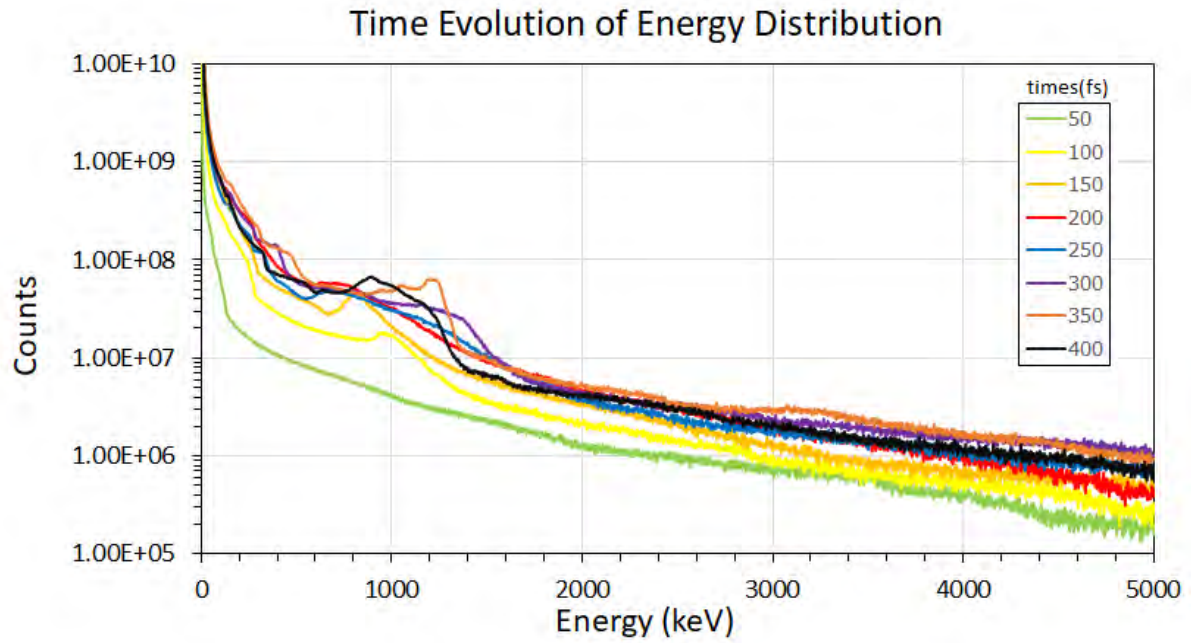


Fig 5.14C Time evolution of energy distribution from 50 to 400 fs for LWFA with plasma density $7 \times 10^{24} \text{ m}^{-3}$ and laser strength $A=10.0$.

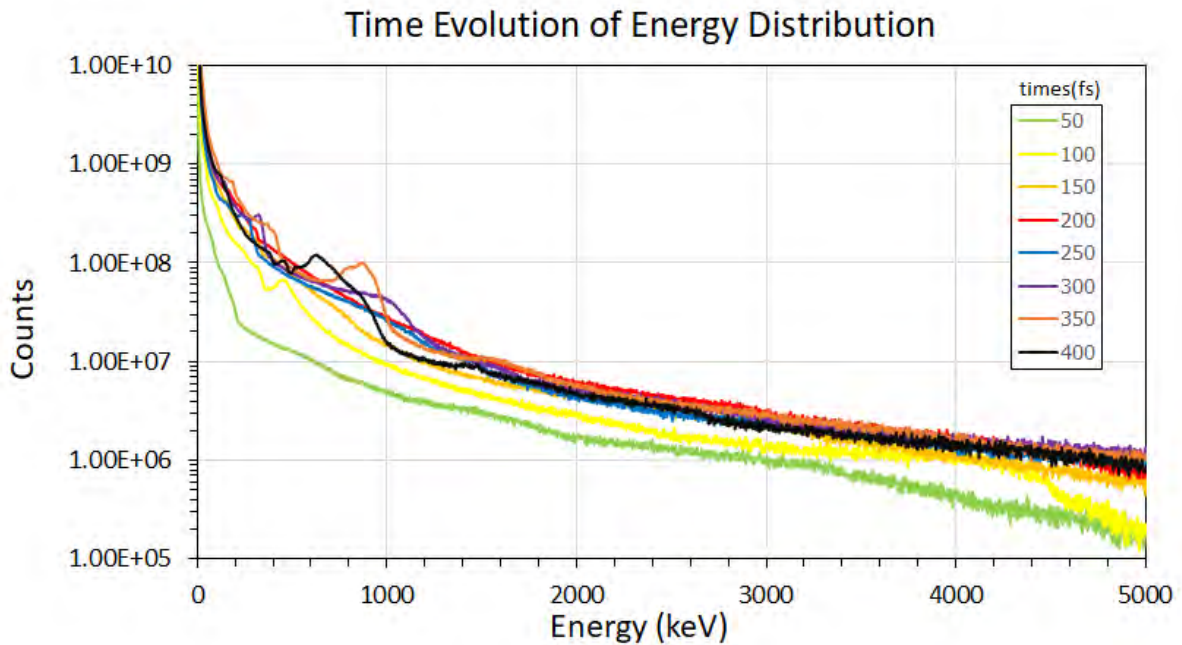


Fig 5.14D Time evolution of energy distribution from 50 to 400 fs for LWFA with plasma density $1 \times 10^{25} \text{ m}^{-3}$ and laser strength $A=10.0$.

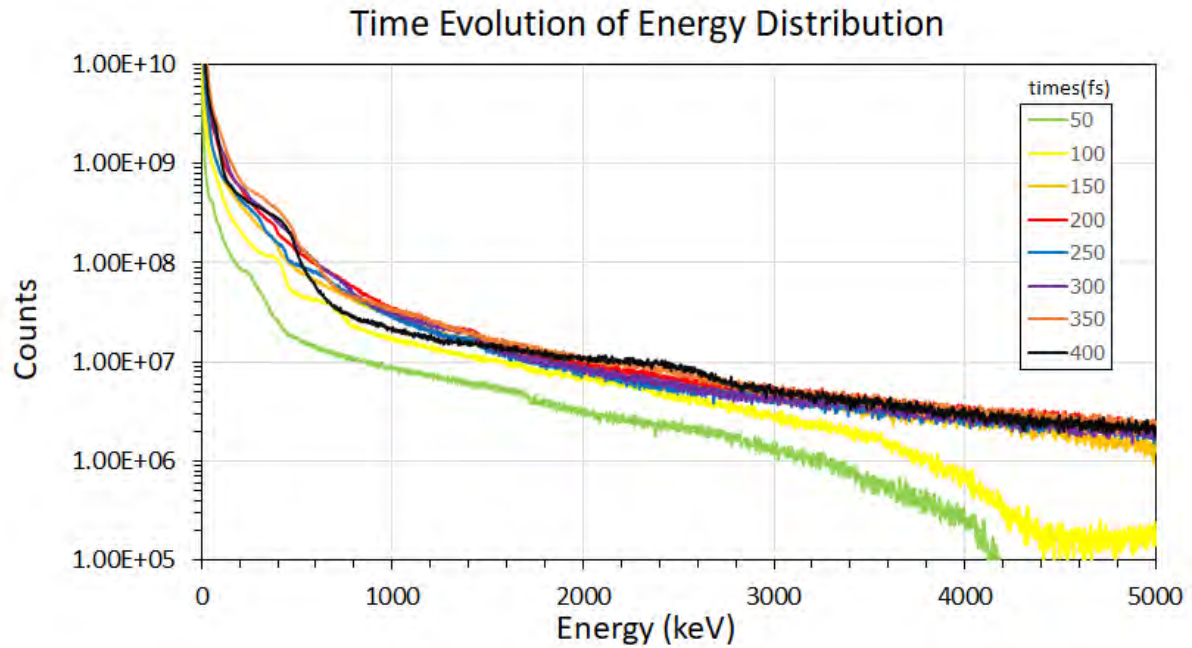


Fig 5.14E Time evolution of energy distribution from 50 to 400 fs for LWFA with plasma density $2 \times 10^{25} \text{ m}^{-3}$ and laser strength $A=10.0$.

Fig. 5.14 shows conclusive evidence that the peak that occurs in lower energy for higher plasma density is the direct result from peak generation at different energy for each plasma density. Higher plasma density tends to create energy peak at lower energy. The deceleration of electrons occurs but does not contribute much to the decrease of peak energy. Moreover, the results show common characteristics as in Fig. 5.14, that peak energy is at the highest value for 300 fs then decreases afterward. Another thing to mention is peak deceleration is higher for lower plasma density. Peak energy decreases from 3800 keV to 2400 keV in time interval between 300 fs and 400 fs for density $2 \times 10^{24} \text{ m}^{-3}$, while peak energy decreases from 1000 to 600 keV for $1 \times 10^{25} \text{ m}^{-3}$ in the same interval, and energy decreases in peak for density $2 \times 10^{25} \text{ m}^{-3}$ is much smaller.

5.4 Axial Magnetic field's influence on electron acceleration

Research found that electrons acceleration is enhanced when there is some value of magnetic field direct in direction of laser propagation. Magnetic field of 10^{-3} , 1 and 10^3 Tesla are implemented for wakefield accelerator at $A=10.0$ and plasma density 10^{25} m^{-3} .

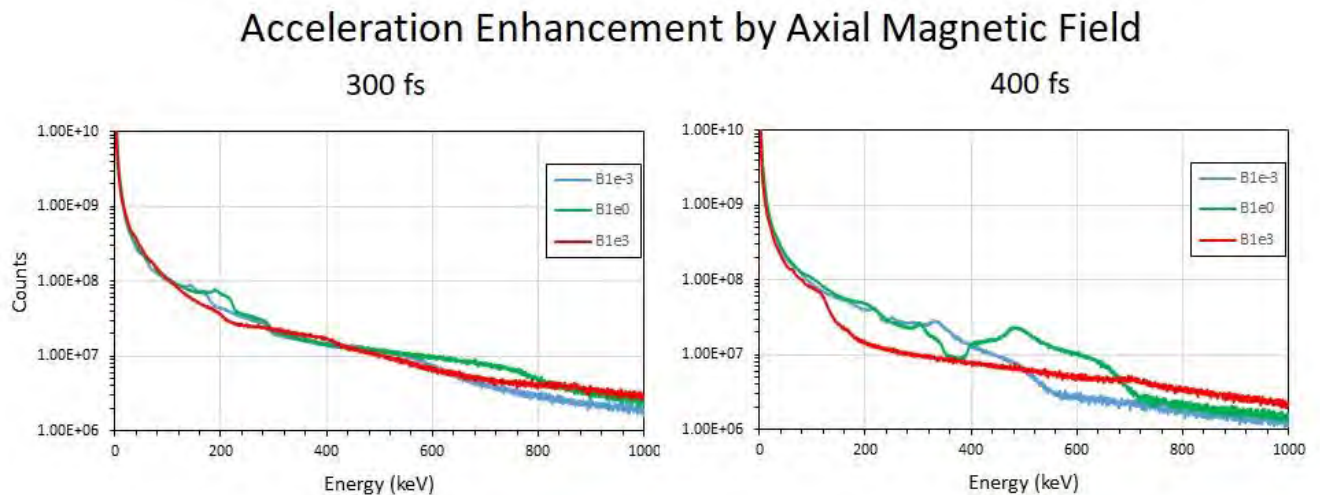


Fig 5.15 Acceleration enhancement by axial magnetic field

Energy distribution at time 300 and 400 fs are plotted in Fig.5.15 for $A=10.0$ and plasma density 10^{25} m^{-3} . At 300 fs, small peaks occur at 200 keV for magnetic field magnitude 1.0 and 10^{-3} Tesla. The difference in energy distribution is negligible. However, at 400 fs, the energy distributions exhibit some differences in electron acceleration.

For time 400 fs, at axial magnetic field of magnitude 10^3 tesla, distribution peak occurs at 720 keV. However, particle count for magnetic magnitude of 1 tesla at 480 keV peak is higher. For magnetic field magnitude 10^3 tesla, there is an evidence that distributions peaks in 400 fs and 300 fs are the results of acceleration. Consider the peak at 300 fs, $B1e3$ 200 keV peaks at 8×10^7 particles which is 2×10^7 higher than $B1e-3$ which is approximately 6×10^7 particles. At 400 fs, $B1e3$'s 480 keV peaks at 3×10^7 particles and $B1e-3$ peaks at 8×10^6 particles. The difference in particles at two different times is approximately the same, about 2×10^7 particles. The excessive number could come from electron trapping and the translation of peaks is a direct result of acceleration. Another thing to mention is differences in acceleration power. The peak of $B1e0$ translates from 200 keV at 300 fs to 480 keV at 400 fs while $B1e-3$ translates its peak from 200 to 320 keV in the same time interval. This difference shows that some values of magnetic field are more appropriate to enhance plasma wakefield accelerator.

The consequence of identifying trapping peak in electron energy distribution is that some plasma density values are more effective for accelerating and trapping electron according to Fig. 5.8. The plasma

density of value 10^{25} m^{-3} enable some processes to make a portion of electrons into the peak at 400 and 1000 keV.

5.5 Discussion

The results and conclusions reached in section 5.1 – 5.4 can be improved in various aspects. First, the information used to probe electrons acceleration can be improved by utilizing data on phase space or value of electromagnetic field inside plasma volume, however, the data comes in form of HDF5 which requires some knowledge to manipulate or extract the information. The memory required to store those data is approximately 25 GB, 800 MB from phase space and 24 GB from field information, for each storing time step. The memory requirement for data of one subgraph of Fig 4.14 will increase at least 200 GB which accounts for only 8 captured timesteps while the study collect the data for every 10 fs. One drawback for not using field quantities in HDF5 is no clarification on pump depletion of laser. The depletions can be investigated through density plot as well, however, the magnitudes of laser's strength are measured and collected in HDF5 format. Utilizing field quantities will help determine pump depletion length that can be compared to the theory. Second, this study uses PConGPU with moderate settings such as medium level of interpolation to lower memory usage of simulation. Full performance simulation cannot be done in NARIT's CHALAWAN because of limited memory that is considered very large compared to personal computer. The simulation can reproduce some phenomenon of wakefield accelerator, however, in the full performance settings, difference may be found. Further study should include the full performance settings, analysis of phase space and field, and more quantitative analysis.

Another thing that should be further investigated is the mixing effect between plasma density and background magnetic field which, in some case, may result in better enhancing performance of LWFA's. Due to incident of COVID-19, the migration to hometown put the project on hiatus because of unreliability of internet connection in the countryside. If there were any synergy, the search for optimum condition for better enhancement would provide more complete conclusion to this study.

5.6 Summary

This senior project on plasma density effect on laser-type plasma wakefield accelerator is conducted by the investigation of particle density plot and energy distribution of particles. The systems of LWFA are simulated using PConGPU program which is developed and maintained by the Junior Group Computational Physics at the Institute for Radiational Physics at Helmholtz Zentrum Dresden Rossendorf (HZDR). The simulation contains $256 \times 2048 \times 256$ grid boxes of sizes are 40 nm in x and z directions and 200 nm in y direction. The simulation volume is $51.2 \mu\text{m} \times 81.92 \mu\text{m} \times 51.2 \mu\text{m}$ and it consists of electrons and protons of equal numbers. The plasma used in our study is hydrogen plasma. The results show that PConGPU can reproduce wakefield phenomenon such as electron blowout, electrons acceleration and self-injection.

The investigations of plasma density effects on LWFA using only energy distributions and particle density plots can be expanded into 4 topics. First topic is about electron and ion motion inside LWFA. From the density plot of electrons and protons, generation of plasma wakefield can be observed. Density plot is also consistent with theoretical characteristic of pondermotive force. Laser's pondermotive force on charge particles is inversely proportional to their mass. Conclusive evidence is presented in Fig. 5.1 where electrons are more affected by laser than are protons. While electrons are blown away from the laser path, proton's density stays approximately unchanged. Behind the laser pulse, positive space charge forms up from the blowout of electrons while protons stay fixed. Electron's energy distribution also shows number of particle peak at a specific value of energy which indicates special motion of electrons. This peak should be due to electron trapping of plasma wake. Second topic is about plasma wake's shape and blowout radius. As plasma density increases, blowout radius and wake's length become smaller as the result of increase in attractive force from positive space charge behind the laser pulse. Moreover, plasma density does not constantly decrease the blowout radius as clarified in Fig. 5.6. The relation between blowout radius and plasma density are qualitatively not the same for all laser strength. This trend is also affected by laser strength too. Laser strengths determine the mode of electron blowout. As in Fig. 5.6, blowout radius variations over plasma density are qualitatively the same for laser strength parameter $A = 5.0$ and 10.0 , complete electron blowout, while $A=1.0$ differs from the other as a result of incomplete blowout. This result strongly agrees with Wei Lu (4) that complete blowout occurs for $A > 2$. The third topic is plasma density effect on electron acceleration. Fig. 5.8 shows the abnormality in energy distribution for plasma density of 10^{25} m^{-3} which is qualitatively different from the others. The investigation for plasma density near 10^{25} m^{-3} is conducted. The results show that some range of plasma density value allows electron trapping which is identified by peak in Fig 5.13 - 5.14. Energy peaks situate at lower energy for higher plasma density as the generation of peaks for higher plasma density is at lower energy. Electron deceleration of peak occurs at approximately 300 fs and the deceleration is less for higher plasma density. The final topic investigated

in this study is magnetic field effect on the energy distribution. The results in Fig. 5.15 shows that for a specific LWFA setting some range of axial magnetic magnitude can be used to enhance electron trapping and create high energy peak. The results also show that too strong magnetic field will suppress the enhancement.

APPENDIX A: Example of .param file

A.1 laser.param

```
/* Copyright 2013-2018 Axel Huebl, Anton Helm, Rene Widera, Richard Pausch, Alexander Debus
```

```
*
```

```
* This file is part of PConGPU.
```

```
*
```

```
* PConGPU is free software: you can redistribute it and/or modify
```

```
* it under the terms of the GNU General Public License as published by
```

```
* the Free Software Foundation, either version 3 of the License, or
```

```
* (at your option) any later version.
```

```
*
```

```
* PConGPU is distributed in the hope that it will be useful,
```

```
* but WITHOUT ANY WARRANTY; without even the implied warranty of
```

```
* MERCHANTABILITY or FITNESS FOR A PARTICULAR PURPOSE. See the
```

```
* GNU General Public License for more details.
```

```
*
```

```
* You should have received a copy of the GNU General Public License
```

```
* along with PConGPU.
```

```
* If not, see <http://www.gnu.org/licenses/>.
```

```
*/
```

```
/** @file
```

```
*
```

```
* Configure laser profiles. All laser propagate in y direction.
```

```
*
```

```

* Available profiles:

* - None          : no laser init

* - GaussianBeam  : Gaussian beam (focusing)

* - PulseFrontTilt : Gaussian beam with a tilted pulse envelope

*                in 'x' direction

* - PlaneWave     : a plane wave (Gaussian in time)

* - Wavepacket    : wavepacket (Gaussian in time and space, not
*                focusing)

* - Polynom       : a polynomial laser envelope

* - ExpRampWithPrepulse : wavepacket with exponential upramps and prepulse

*

* In the end, this file needs to define a 'Selected' class in namespace
* `picongpu::fields::laserProfiles`. A typical profile consists of a
* laser profile class and its parameters. For example:

*
* @code{.cpp}
* using Selected = GaussianBeam< GaussianBeamParam >;
* @endcode
*/

#pragma once

#include "picongpu/fields/laserProfiles/profiles.def"

#ifdef PARAM_A0

```

```

# define PARAM_A0 8.0

#endif

#ifndef PARAM_WAVE_LENGTH_SI
# define PARAM_WAVE_LENGTH_SI 0.8e-6

#endif

#ifndef PARAM_PULSE_LENGTH_SI
# define PARAM_PULSE_LENGTH_SI 5.e-15

#endif

namespace picongpu
{
namespace fields
{
namespace laserProfiles
{
namespace gaussianBeam
{
//! Use only the 0th Laguerremode for a standard Gaussian
static constexpr uint32_t MODENUMBER = 0;

PMACC_CONST_VECTOR(float_X, MODENUMBER + 1, LAGUERREMODES, 1.0);

// This is just an example for a more complicated set of Laguerre modes
//constexpr uint32_t MODENUMBER = 12;

```

```

//PMACC_CONST_VECTOR(float_X, MODENUMBER + 1, LAGUERREMODES, -1.0, 0.0300519, 0.319461, -
0.23783, 0.0954839, 0.0318653, -0.144547, 0.0249208, -0.111989, 0.0434385, -0.030038, -0.00896321, -
0.0160788);

} // namespace gaussianBeam

struct GaussianBeamParam
{
    /** unit: meter */

    static constexpr float_64 WAVE_LENGTH_SI = PARAM_WAVE_LENGTH_SI;

    /** Convert the normalized laser strength parameter a0 to Volt per meter */

    static constexpr float_64 UNITCONV_A0_to_Amplitude_SI = -2.0 * PI / WAVE_LENGTH_SI *
::picongpu::SI::ELECTRON_MASS_SI * ::picongpu::SI::SPEED_OF_LIGHT_SI * ::picongpu::SI::SPEED_OF_LIGHT_SI
/ ::picongpu::SI::ELECTRON_CHARGE_SI;

    /** unit: W / m^2 */

    // calculate: _A0 = 8.549297e-6 * sqrt( Intensity[W/m^2] ) * wavelength[m] (linearly polarized)

    /** unit: none */

    static constexpr float_64 _A0 = PARAM_A0;

    /** unit: Volt / meter */

    static constexpr float_64 AMPLITUDE_SI = _A0 * UNITCONV_A0_to_Amplitude_SI;

    /** unit: Volt / meter */

```

```

//static constexpr float_64 AMPLITUDE_SI = 1.738e13;

/** Pulse length: sigma of std. gauss for intensity (E^2)

* PULSE_LENGTH_SI = FWHM_of_Intensity / [ 2*sqrt{ 2* ln(2) } ]

*           [ 2.354820045 ]

* Info:      FWHM_of_Intensity = FWHM_Illumination

*           = what a experimentalist calls "pulse duration"

*

* unit: seconds (1 sigma) */

static constexpr float_64 PULSE_LENGTH_SI = PARAM_PULSE_LENGTH_SI;

/** beam waist: distance from the axis where the pulse intensity (E^2)

*           decreases to its 1/e^2-th part,

*           at the focus position of the laser

* W0_SI = FWHM_of_Intensity / sqrt{ 2* ln(2) }

*           [ 1.17741 ]

*

* unit: meter */

static constexpr float_64 W0_SI = 5.0e-6 / 1.17741;

/** the distance to the laser focus in y-direction

* unit: meter */

static constexpr float_64 FOCUS_POS_SI = 4.62e-5;

/** The laser pulse will be initialized PULSE_INIT times of the PULSE_LENGTH

*

```

```

* unit: none */

static constexpr float_64 PULSE_INIT = 15.0;

/** cell from top where the laser is initialized
*
* if `initPlaneY == 0` than the absorber are disabled.
* if `initPlaneY > absorbercells negative Y` the negative absorber in y
* direction is enabled
*
* valid ranges:
* - initPlaneY == 0
* - absorber cells negative Y < initPlaneY < cells in y direction of the top gpu
*/

static constexpr uint32_t initPlaneY = 0;

/** laser phase shift (no shift: 0.0)
*
* sin(omega*time + laser_phase): starts with phase=0 at center --> E-field=0 at center
*
* unit: rad, periodic in 2*pi
*/

static constexpr float_X LASER_PHASE = 0.0;

using LAGUERREMODES_t = gaussianBeam::LAGUERREMODES_t;

static constexpr uint32_t MODENUMBER = gaussianBeam::MODENUMBER;

```

```

/** Available polarisation types
 */

enum PolarisationType
{
    LINEAR_X = 1u,
    LINEAR_Z = 2u,
    CIRCULAR = 4u,
};

/** Polarization selection
 */

static constexpr PolarisationType Polarisation = CIRCULAR;

};

//! currently selected laser profile

using Selected = GaussianBeam<GaussianBeamParam>;

} // namespace laserProfiles

} // namespace fields

} // namespace picongpu

```

A.2 density.param

```

/* Copyright 2013-2018 Axel Huebl, Rene Widera, Felix Schmitt,
 *
 *          Richard Pausch, Marco Garten
 *
 *
 * This file is part of PICongGPU.

```

*

* PIconGPU is free software: you can redistribute it and/or modify
* it under the terms of the GNU General Public License as published by
* the Free Software Foundation, either version 3 of the License, or
* (at your option) any later version.

*

* PIconGPU is distributed in the hope that it will be useful,
* but WITHOUT ANY WARRANTY; without even the implied warranty of
* MERCHANTABILITY or FITNESS FOR A PARTICULAR PURPOSE. See the
* GNU General Public License for more details.

*

* You should have received a copy of the GNU General Public License
* along with PIconGPU.
* If not, see <<http://www.gnu.org/licenses/>>.

*/

```
#pragma once
```

```
#include "picongpu/particles/densityProfiles/profiles.def"
```

```
/* preprocessor struct generator */
```

```
#include <pmacc/preprocessor/struct.hpp>
```

```
namespace picongpu
```

```
{
```

```
namespace SI
```



```

{

/** Base density in particles per m^3 in the density profiles.

*

* This is often taken as reference maximum density in normalized profiles.

* Individual particle species can define a `densityRatio` flag relative

* to this value.

*

* unit: ELEMENTS/m^3

*/

#ifndef PARAM_BASE_DENSITY_SI
# define PARAM_BASE_DENSITY_SI 1.e22
#endif

constexpr float_64 BASE_DENSITY_SI = PARAM_BASE_DENSITY_SI;
}

namespace densityProfiles
{

PMACC_STRUCT(GaussianParameter,

/** Profile Formula:

* constexpr float_X exponent = abs((y - gasCenter_SI) / gasSigma_SI);

* constexpr float_X density = exp(gasFactor * pow(exponent, gasPower));

*

* takes `gasCenterLeft_SI` for  $y < \text{gasCenterLeft\_SI}$ ,

* `gasCenterRight_SI` for  $y > \text{gasCenterRight\_SI}$ ,

* and exponent = 0.0 for  $\text{gasCenterLeft\_SI} < y < \text{gasCenterRight\_SI}$ 

```

```

*/

(PMACC_C_VALUE(float_X, gasFactor, -1.0))

(PMACC_C_VALUE(float_X, gasPower, 4.0))

/** height of vacuum area on top border

*

* this vacuum is important because of the laser initialization,

* which is done in the first cells of the simulation and

* assumes a charge-free volume

* unit: cells

*/

(PMACC_C_VALUE(uint32_t, vacuumCellsY, 50))

/** The central position of the gas distribution

* unit: meter

*/

(PMACC_C_VALUE(float_64, gasCenterLeft_SI, 8.0e-5))

(PMACC_C_VALUE(float_64, gasCenterRight_SI, 15.0e-5))

/** the distance from gasCenter_SI until the gas density decreases to its 1/e-th part

* unit: meter

*/

(PMACC_C_VALUE(float_64, gasSigmaLeft_SI, 8.0e-5))

(PMACC_C_VALUE(float_64, gasSigmaRight_SI, 8.0e-5))

); /* struct GaussianParam */

```

```
/* definition of density with Gaussian profile */  
  
using Gaussian = GaussianImpl< GaussianParameter >;  
  
}  
  
}
```

A.3 grid.param

```
/* Copyright 2013-2018 Axel Huebl, Rene Widera, Benjamin Worpitz  
  
*  
  
* This file is part of PICongPU.  
  
*  
  
* PICongPU is free software: you can redistribute it and/or modify  
* it under the terms of the GNU General Public License as published by  
* the Free Software Foundation, either version 3 of the License, or  
* (at your option) any later version.  
  
*  
  
* PICongPU is distributed in the hope that it will be useful,  
* but WITHOUT ANY WARRANTY; without even the implied warranty of  
* MERCHANTABILITY or FITNESS FOR A PARTICULAR PURPOSE. See the  
* GNU General Public License for more details.  
  
*  
  
* You should have received a copy of the GNU General Public License  
* along with PICongPU.  
  
* If not, see <http://www.gnu.org/licenses/>.  
  
*/
```

```

#pragma once

namespace picongpu
{

namespace SI
{

/** Duration of one timestep
 * unit: seconds */
constexpr float_64 DELTA_T_SI = 1.e-16;

/** equals X
 * unit: meter */
constexpr float_64 CELL_WIDTH_SI = 0.20e-6;

/** equals Y - the laser & moving window propagation direction
 * unit: meter */
constexpr float_64 CELL_HEIGHT_SI = .40e-7;

/** equals Z
 * unit: meter */
constexpr float_64 CELL_DEPTH_SI = CELL_WIDTH_SI;

/** Note on units in reduced dimensions
 *

```

```

* In 2D3V simulations, the CELL_DEPTH_SI (Z) cell length
* is still used for normalization of densities, etc.
*
* A 2D3V simulation in a cartesian PIC simulation such as
* ours only changes the degrees of freedom in motion for
* (macro) particles and all (field) information in z
* travels instantaneous, making the 2D3V simulation
* behave like the interaction of infinite "wire particles"
* in fields with perfect symmetry in Z.
*/
} //namespace SI

//! Defines the size of the absorbing zone (in cells)
constexpr uint32_t ABSORBER_CELLS[3][2] = {
    {32, 32}, /*x direction [negative,positive]*/
    {32, 32}, /*y direction [negative,positive]*/
    {32, 32} /*z direction [negative,positive]*/
}; //unit: number of cells

//! Define the strength of the absorber for any direction
constexpr float_X ABSORBER_STRENGTH[3][2] = {
    {1.0e-3, 1.0e-3}, /*x direction [negative,positive]*/
    {1.0e-3, 1.0e-3}, /*y direction [negative,positive]*/
    {1.0e-3, 1.0e-3} /*z direction [negative,positive]*/
}; //unit: none

```

```

constexpr uint32_t ABSORBER_FADE_IN_STEPS = 16;

/** When to move the co-moving window.
 *
 * An initial pseudo particle, flying with the speed of light,
 *
 * is fired at the begin of the simulation.
 *
 * When it reaches movePoint % of the absolute(*) simulation area,
 *
 * the co-moving window starts to move with the speed of light.
 *
 *
 * (*) Note: beware, that there is one "hidden" row of gpus at the y-front,
 *
 *      when you use the co-moving window
 *
 * 0.75 means only 75% of simulation area is used for real simulation
 */
constexpr float_64 movePoint = 0.8;

}

```

APPENDIX B: Example of .cfg file

```

# Copyright 2013-2018 Axel Huebl, Rene Widera, Felix Schmitt

#

# This file is part of PICongPU.

#

# PICongPU is free software: you can redistribute it and/or modify
# it under the terms of the GNU General Public License as published by
# the Free Software Foundation, either version 3 of the License, or
# (at your option) any later version.

```

```
#

# PIconGPU is distributed in the hope that it will be useful,

# but WITHOUT ANY WARRANTY; without even the implied warranty of

# MERCHANTABILITY or FITNESS FOR A PARTICULAR PURPOSE. See the

# GNU General Public License for more details.

#

# You should have received a copy of the GNU General Public License

# along with PIconGPU.

# If not, see <http://www.gnu.org/licenses/>.

#

##

## This configuration file is used by PIconGPU's TBG tool to create a

## batch script for PIconGPU runs. For a detailed description of PIconGPU

## configuration files including all available variables, see

##

##          docs/TBG_macros.cfg

##

#####

## Section: Required Variables ##

#####

TBG_wallTime="6:00:00"
```

TBG_devices_x=1

TBG_devices_y=2

TBG_devices_z=1

TBG_gridSize="192 2000 192"

TBG_steps="1000"

TBG_periodic="--periodic 1 0 1"

TBG_movingWindow="-m"

TBG_windowMovePoint="--windowMovePoint 0.90 "

TBG_stopWindow="--stopWindow 1000"

#####

Section: Optional Variables

#####

png image output (rough electron density and laser preview)

TBG_pngYX="--e_png.period 50 \

--e_png.axis yx --e_png.slicePoint 0.5 \

--e_png.folder pngElectronsYX"

TBG_ionpngYX="--i_png.period 100 \

--i_png.axis yx --i_png.slicePoint 0.5 \

--i_png.folder pngElectronsYX"


```

# energy histogram (electrons, [keV])

TBG_e_histogram="--e_energyHistogram.period 50 \

    --e_energyHistogram.binCount 2048 \

    --e_energyHistogram.minEnergy 0 --e_energyHistogram.maxEnergy 20000 \

    --e_energyHistogram.filter all"

# longitudinal phase space (electrons, [m_e c])

TBG_e_PSyPy="--e_phaseSpace.period 100 \

    --e_phaseSpace.space y --e_phaseSpace.momentum py \

    --e_phaseSpace.min -1.0 --e_phaseSpace.max 1.0 \

    --e_phaseSpace.filter all"

# HDF5 raw data output (DISABLED, add to TBG_plugins below to ENABLE!)

TBG_hdf5="--hdf5.period 100 \

    --hdf5.file simData \

    --hdf5.source 'species_all,fields_all'"

# macro particle counter (electrons, debug information for memory)

TBG_e_macroCount="--e_macroParticlesCount.period 100"

# Calorimeter

TBG_e_Calorimeter="--e_calorimeter.period 100 \

    --e_calorimeter.file ecalorimeter \

    --e_calorimeter.filter all \

```

```

--e_calorimeter.logScale 0 \
"
TBG_plugins="!TBG_pngYX \
!TBG_ionpngYX \
!TBG_e_histogram \
!TBG_e_PSyPy \
!TBG_e_macroCount \
!TBG_hdf5 \
!TBG_e_Calorimeter"
#Add more plugins Particle calories meter, slice field, count particles

#####

## Section: Program Parameters ##

#####

TBG_deviceDist="!TBG_devices_x !TBG_devices_y !TBG_devices_z"

TBG_programParams="-d !TBG_deviceDist \
-g !TBG_gridSize \
-s !TBG_steps \
!TBG_movingWindow \
!TBG_periodic \
!TBG_plugins \
--versionOnce"

```

```
# TOTAL number of devices
```

```
TBG_tasks=$(( TBG_devices_x * TBG_devices_y * TBG_devices_z ))
```

```
"$TBG_cfgPath"/submitAction.sh
```

Bibliography

1. *On the origin of the cosmic radiation.* **E., Fermi.** 8, Physical Review, Vol. 75, pp. 1169-1174. 0031899X (ISSN).
2. *Interaction of relativistic particles and free electromagnetic waves in the presence of a static helical magnet.* **Palmer, R. B.** 7, 1972, J Appl Phys, Vol. 43, pp. 3014-3023.
3. *Ultra-high gradient particle acceleration by intense laser-driven plasma density waves.* **Joshi, C. et al.** 5986, 1984, Nature, Vol. 311, pp. 525-529. 00280836 (ISSN).
4. **Lu, Wei.** Nonlinear Plasma Wakefield Theory and Optimum Scaling for Laser Wakefield Accelerator (LWFA) in the Blowout Regime. *Dissertation.* 2006.
5. *Theory of motion wave of electron plasma.* **Polovin, A. I Akhiezer and R. V.** 30, 1956, JETP(U.S.S.R.), pp. 915-928.
6. *Laser electron accelerator.* **Tajima, T. and Dawson, J. M.** 4, 1979, Physical Review Letters, Vol. 43, pp. 267-270. 00319007 (ISSN).
7. *Unlimited electron acceleration in laser-driven plasma waves.* **Katsouleas, T. and Dawson, J. M.** 5, Physical Review Letters, Vol. 51, pp. 392-395. 00319007 (ISSN).
8. *Enhanced electron trapping by a static longitudinal magnetic field in laser wakefield acceleration.* **Hur, M. S.** 15, 2008, Physics Letters, Section A: General, Atomic and Solid State Physics, Vol. 372, pp. 2684-2687.
9. *Reshaping of intense laser pulse with a capillary.* **Lihua Cao, Wei Yu, M. Y. Yu, Xin Wang, Yugiu Gu, and X. T. He.** 16, 2009, Physics of Plasmas. 093109.
10. *Laser pulse reshaping with spectral scanning filtering based on optical Kerr effect.* **Rong Ye, Xianyun Wu, Ming Yin.** 2018 : Elsevier, Optik, Vol. 157, pp. 382-387.

11. *Circumventing the Dephasing and Depletion Limits of Laser-Wakefield Acceleration*. Alexander Debus, Richard Pausch, Axel Huebl, Klaus Steiniger, René Widera, Thomas E. Cowan, Ulrich Schramm, and Michael Bussmann. 01328, s.l. : HZDR, Vol. 400.
12. *Particle simulation in Plasma*. Dawson, J. M. 403, 1983, Rev. Mod. Phys., Vol. 55.
13. *Nonlinear Electron Oscillations in a Cold Plasma*. Dawson, J.M. Physical Review, Vol. 113, pp. 383-387.
14. *The plasma wakefield accelerator*. Mori, A., Dawson, J. M., Joshi, C., Katsouleas, T., Su, J. J., Wilks, S. 1988, Proceedings of SPIE - The International Society for Optical Engineering, Vol. 873, pp. 214-222. 0277786X (ISSN).
15. *Physics of laser-driven plasma-based electron accelerator*. E. Esarey, C. B. Schroeder, and W. P. Leemans. s.l. : Review of modern Physics, 2009, Vol. 81.